White Rose Research Online
eprints@whiterose.ac.uk
https://eprints.whiterose.ac.uk
Universities of Leeds, Sheffield and York

Deposited via The University of Leeds.

White Rose Research Online URL for this paper:
https://eprints.whiterose.ac.uk/id/eprint/124826/

Version: Accepted Version

Article:

Yan, N and Baas, ACW (2018) Transformation of parabolic dunes into mobile barchans triggered by environmental change and anthropogenic disturbance. Earth Surface Processes and Landforms, 43 (5). pp. 1001-1018. ISSN: 0197-9337

https://doi.org/10.1002/esp.4299

© 2017 John Wiley & Sons, Ltd.. This is the peer reviewed version of the following article: Yan, N., and Baas, A. C. W. (2018) Transformation of parabolic dunes into mobile barchans triggered by environmental change and anthropogenic disturbance. Earth Surf. Process. Landforms, doi: 10.1002/esp.4299., which has been published in final form at https://doi.org/10.1002/esp.4299. This article may be used for non-commercial purposes in accordance with Wiley Terms and Conditions for Self-Archiving. Uploaded in accordance with the publisher's self-archiving policy.

Reuse
Items deposited in White Rose Research Online are protected by copyright, with all rights reserved unless indicated otherwise. They may be downloaded and/or printed for private study, or other acts as permitted by national copyright laws. The publisher or other rights holders may allow further reproduction and re-use of the full text version. This is indicated by the licence information on the White Rose Research Online record for the item.

Takedown
If you consider content in White Rose Research Online to be in breach of UK law, please notify us by emailing eprints@whiterose.ac.uk including the URL of the record and the reason for the withdrawal request.

UNIVERSITY OF LEEDS
University of Sheffield
UNIVERSITY of York

Title

Transformation of parabolic dunes into mobile barchans triggered by environmental change and anthropogenic disturbance

Authors

Na Yan[1,2] * and Andreas C.W. Baas[1]

[1] Department of Geography, King's College London, UK

[2] School of Earth and Environment, University of Leeds, UK

***Correspondence to:**

Na Yan
School of Earth and Environment
University of Leeds
Leeds
UK
Email: n.yan@leeds.ac.uk

Abstract

Parabolic dunes are widely distributed on coasts and margins of deserts and steppes where ecosystems are valuable and sensitive to environmental changes and human disturbances. Some studies have indicated that vegetated parabolic dunes can be activated into highly mobile barchan dunes and the catastrophic shift of eco-geomorphic systems is detrimental to land management and social-economic development; however, no detailed study has clarified the physical processes and eco-geomorphic interactions that control the stability of a parabolic dune and its resistance to unfavourable environmental changes. This study utilises the Extended-DECAL (Discrete Eco-geomorphic Aeolian Landscapes) model, parameterised by field measurements of dune topography and vegetation characteristics combined with remote sensing, to explore how increases in drought stress, wind strength, and grazing stress may lead to the activation of stabilising parabolic dunes into highly mobile barchans. The modelling results suggest that the mobility of an initial parabolic dune at the onset of a perturbation determines the capacity of a system to absorb environmental change, and a slight increase in vegetation cover of an initial parabolic dune can increase the activation threshold significantly. The characteristics of four eco-geomorphic interaction zones control the processes and resulting morphologies of the transformations. A higher deposition tolerance of vegetation increases the activation threshold of the climatic impact and sand transport rate, whereas the erosion tolerance of vegetation influences the patterns of resulting barchans (a single barchan vs. multiple barchans). The change in the characteristics of eco-geomorphic interaction zones may indirectly reflect the dune stability and predict an ongoing transformation, whilst the activation angle may be potentially used as a proxy of environmental stresses. In contrast to the natural environmental changes that tend to affect relatively weak and young plants, grazing stress can exert a broader impact on any plant indistinctively. A small increase in grazing stress just above the activation threshold can accelerate dune activation significantly.

Keywords

Dune activation; water stress; wind strength; overgrazing; eco-geomorphic interaction

1. Introduction

Parabolic dunes typically have a U- or V- shaped lobe with two trailing arms pointing upwind, although they may develop more complicated morphologies, e.g., digitated and rake-like parabolic dunes, under the controls of wind regime, sediment supply and vegetation characteristics (Pye and Tsoar, 1990; Rubin and Hunter, 1987; Wasson and Hyde, 1983; Yan *et al.*, 2010). They have been found prevalent around the world, on coasts, river valleys, lakeshores, and margins of deserts and steppes (Yan and Baas, 2015). Controlled by different wind regime, vegetation cover, and sediment supply, the migration rate of active parabolic dunes varies substantially from 0.05 m yr^{-1} in Northern Australia (Story, 1982) to as fast as 80 m yr^{-1} in Manawatu (Hesp, 2001), and their planform morphologies vary broadly from lunate, hemicyclic, to elongated shapes with an increase of the length to width ratio (from <1 to >3). In particular, some parabolic dunes on the east coast of Queensland in Australia develop a length to width ratio larger than 6 with trailing arms extending thousands of meters (Pye, 1982). Parabolic dunes are, however, usually relative low in height, limited to the scale of meters to tens of meters (Goudie, 2011). The morphology, distribution, and migration rate of parabolic dunes around the world have been fully reviewed and summarised in Yan and Baas (2015). Parabolic dunes can develop from the stabilisation of mobile barchan and transverse dunes under ameliorating vegetation conditions (McKee, 1966; Stetler and Gaylord, 1996; Tsoar and Blumberg, 2002), or from the extension of blowouts in coastal foredunes when vegetation cover undergoes natural or anthropogenic disturbances, e.g., wildfires, storms, overgrazing, and trampling (Carter *et al.*, 1990; Hesp, 2001; Muckersie and Shepherd, 1995). Initially active parabolic dunefields can become fully stabilised over time, entirely covered with vegetation and so-called ‘dormant’. Many studies now exist on attempts at re-activating such dormant parabolic dunes, in order to recover the more dynamic and ecologically rich environments of active sand drifts (e.g., Arens *et al.*, 2004). Going one step further, however, two studies also report the transformation from active parabolic dunes into bare-sand barchans and transverse dunes as a consequence of decline in precipitation (Schulmeister and Lees, 1992, pp. 532-533), or as a result of anthropogenic stresses such as increased aboriginal burning and grazing (Hesp 2001, pp. 38). Similarly, Anton and Vincent (1986) report the development of (bare-sand) domical dunes from the detachment of parabolic dune noses from their arms on sabkhas where vegetation is limited by salinity conditions (pp. 192), and they also report isolated barchanoid features developing inside the parabolic dune fields of the Jafurah Desert (pp. 191). While a sizeable literature exists both on the stabilisation of barchans into parabolic dunes as well as on contemporary re-activation of dormant parabolic dunefields, there are no direct studies of the (re-)emergence of barchans from parabolic dunes, even though this transformation type has clearly significant implications for land management and socio-economic resource, particularly under climatic change. The study we present here attempts to investigate the eco-geomorphic dynamics of such a dune transformation, from parabolic to barchan, by means of simulations with a well-established computer model.

Computer modelling of aeolian landscapes and sand transport processes has been in wide use over the past few decades, due to its capability of bridging the gap between different temporal and spatial scales (Werner, 1995; 1999). Numerical simulations serve as an important tool to interpret field data and phenomena observed, to investigate theoretical foundations underlying distinctive landscape patterns, to elucidate possible landscape evolutions and threshold sensitivities, to explore responses to perturbations arising from both natural and anthropogenic impacts, and to assist in understanding complex system behaviour and planning land management.

Within the context of climate change, the aim of this study is to understand the fundamental mechanisms and eco-geomorphic interactions that drive the re-activation and transformation of partially-stabilised parabolic dunes into highly mobile barchan dunes, achieved through Cellular Automaton (CA) computer simulation modelling that is informed by real-world data from fieldwork investigations and remote sensing imagery. Three most common activation mechanisms are explored, including drought stress, increasing wind strength, and overgrazing impact. We investigate in detail the influence of vegetation characteristics and the bare surface fraction of an initial parabolic dune on the transformation thresholds of these activation mechanisms. The model simulations are conducted in the context of a real-world study region, the inland parabolic dunes of the Hobq Desert on the Ordos Plateau of Inner Mongolia, China, described in full in Yan and Baas (2017).

2. Methodology

2.1. Algorithm

The model extends DECAL, the Discrete ECo-geomorphic Aeolian Landscapes model of Nield and Baas (2008). Itself based on an algorithm by Werner (1995), dune topography developing by wind is represented on a gridded domain by accumulations of discreet sand slabs, which are individually picked up, moved in one direction by wind, and deposited on destination cells, with stochastic controls. The transport process is modulated by a ‘shadow zone’ sediment sink in the shelter of dunes, where slabs build a slip face and cannot be eroded, and a domain-wide maintenance of the angle of repose for loose sand by avalanching. As with the prior modelling study (Yan and Baas 2017), the spatial resolution of the domain is set at 1 × 1 m^2 to represent the growth of individual shrubs of Ordos Sagebrush (*Artemisia ordosica*), the principal vegetation of the study region, to ensure sufficient detail in topography and vegetation patterns. Plants in the domain are represented by a vegetation effectiveness, ρ, on each cell, capturing the capability of vegetation to reduce sand transport by altering local erosion and deposition probabilities. Vegetation effectiveness is linked to ground cover and varies over its physiological range [$\rho_{physioMin}$, $\rho_{physioMax}$], with a negative value denoting plants not yet large enough to impede any sand transport, while $\rho > 1$ allows vegetation to grow beyond the density or coverage threshold that entirely stops sand transport. Decline or growth of the plants in response to erosion and burial by sand slabs is modelled with a growth function. While the original DECAL growth functions are static and simulate homogenous ground cover like grasses, the Extended DECAL algorithm used in the study here employs a 'dynamic growth function' simulating clump-like perennials, such as Ordos Sagebrush, whose growth is age-dependent and is sensitive to changes in short-term seasonality and climatic fluctuations, long-term climatic changes, and anthropogenic forces. First, a shrub seed can only germinate on bare surfaces under near-neutral sedimentation balance (0 - 0.1 m $season^{-1}$) (Kobayashi *et al.,* 1995). Then, its growth is seasonal: in growing seasons (Spring & Summer), a shrub grows at a maximum growth rate of α under a neutral sedimentation balance, and reduced in proportion with either erosion or sand burial. When erosion or burial exceeds the erosion tolerance (τ_{eroMax}) or the deposition tolerance (τ_{depMax}), respectively, the plant is entirely removed by uprooting or complete burial. Meanwhile, as a shrub grows in size, it has a greater tolerance to both erosion and sand burial events, and its impact on sand transport is amplified. In non-growing seasons (Autumn & Winter), a shrub sheds its leaves, resulting in a reduced interference of sediment transport.

As most shrubs have different capabilities of growth and response to erosion and deposition at different stages of their life cycle, τ_{eroMax} and τ_{depMax} are determined each season by scaling the existing ρ in a cell against two fundamental shrub parameters, the physiological erosion tolerance ($\tau_{E\_physioMax}$) and deposition tolerance ($\tau_{D\_physioMax}$) properties, defined as the sedimentation tolerances when the plant is at $\rho_{physioMax}$. The maximum growth rate α for a shrub at a specific age is established through a power-law regression relationship between the canopy cover (as a proxy for the effect on reducing sand transport) and the scaled vegetation dimension (as a proxy for the age of a plant) based on empirical data obtained from vegetation measurements in field surveys. The Extended DECAL algorithm summarised above is more fully described in Yan and Baas (2017); in particular, Appendix A in that paper describes in detail how empirical vegetation measurements from the field site in the Hobq Desert were used to establish the power-law relationship between shrub age and vegetation effectiveness that is implemented in the model.

Since the inland parabolic dunes in the study region are fully surrounded by well-vegetated shrub fields, the simulated dunes in this modelling study are treated as isolated systems with sediment being reworked only from the surface of the dunes themselves and/or exhumed from the substratum underneath, without input from an external upwind sediment supply. Analysis of remote sensing imagery sequences in combination with RTK-dGPS surveys in the field yielded an average sand transport rate potential of 20 m^3 m^{-1} yr^{-1} in the study region (see details in Yan and Baas, 2017), which is applied here as the default annual transport rate in the model simulations. The seasonal sand transport regimes are defined as per table 2 of Yan & Baas (2017), using a total of 120 model iterations per year.

Two aspects of the extended algorithm are specifically relevant to the work presented here and were not included in Yan and Baas (2017): relating to climatic impacts and grazing pressure. As mentioned above, α is the growth rate of an individual plant during the growing seasons under its typical climatic conditions in the absence of sedimentation effects. A climatic change leading to a change of water availability can influence the vitality and growth of the plant species. Water availability is particularly crucial to plants in their growing seasons. Therefore, climatic impacts on the vegetation growth are incorporated in the model through a change of the maximum growth rate ($\Delta\alpha_{climate}$) modelled as:

$$\Delta\alpha_{climate} = I_{climate}\, S_{veg}\alpha^{i} \tag{1}$$

where: $I_{climate}$ denotes the climatic impact; S_{veg} denotes the sensitivity of the specific plant species to the climatic impact, [0, 1]; and i is a curve factor dependent on plant species and environmental conditions. A positive climatic impact promotes the growth of vegetation, while a negative climatic impact discourages it.

Overgrazing is also one of the most significant pressures on vegetation in dune systems (Jiang *et al.*, 1995; Ravi *et al.*, 2010; Zheng *et al.*, 2006). The Extended-DECAL simulates an environment where animals are roaming around and consuming a small portion of plant at each stop or time until their demands are satisfied. Forage demand per year (δ), defined in units of vegetation effectiveness ρ in the model, is controlled by the number of livestock, the amount of forage needed per capita per foraging time, and the grazing frequency. Forage demand per iteration (ε) is then expressed as:

$$\varepsilon = \frac{\delta}{\sum_{1}^{n} I_i} \tag{2}$$

where: n is the number of growing seasons per year; and I_i is the number of iterations at the i^{th} growing season. Every grid cell in the modelling domain is assumed to have an equal probability for offering forage to animals. Once a grid cell is randomly selected, it provides animals with a certain amount of vegetation ($\Delta\rho_g$) of its available vegetation as:

$$\Delta\rho_g = \gamma(\rho - \rho_{physioMin}) \quad (3)$$

where: γ is the predefined fraction of a plant consumed by animals at one feeding, 0.05 by default. This process is repeated until the overall vegetation consumed by animals meets the forage demand per iteration (ε). We acknowledge that the grazing algorithm and its assumptions are rather simplistic out of necessity to minimise the number of additional parameters being introduced (requiring justification and sensitivity testing). Nevertheless, it may fairly reflect the random browsing behaviour of livestock (sheep, goats) across a domain of this size (100s of meters) and accumulated over the course of 3-month periods (the modelling seasons).

2.2. Simulation strategy

A simulation of a migrating barchan dune transforming into a parabolic dune under the influence of colonising and stabilising vegetation, presented in Yan and Baas (2017), is used as the basis for selecting different starting points along this timeline for initiating impacts of climatic change and grazing, as indicated in figure 1, that lead to (re-)mobilisation of the parabolic dune lobe and transformation into a barchan dune.

2.2.1. **Water availability**

For decreased water availability, five starting points reflect partially stabilised parabolic dunes with different degrees of bare surface fraction (*BSF*) of the dune surface, calculated from the vegetation effectiveness values within the cells that compose the dune surface above the surrounding plain, as below:

$$BSF = \left(\sum_{i=1}^{n} M_i\right)/n \tag{4}$$

$$M_i = f(\rho) = \begin{cases} 1, & \rho \leq 0 \\ 1-\rho, & 0 < \rho \leq 1 \\ 0, & \rho > 1 \end{cases} \tag{5}$$

Where *n* is the number of cells that are above the surrounding plain. The starting points are at stabilising stages (t_0) of 80, 90, 100, 110, and 120 year, associated with *BSF* levels of 0.34, 0.25, 0.17, 0.06, and 0.00, respectively.

To examine the influence of vegetation properties on the reactivation of the same state of parabolic dunes (i.e. mobility and morphology), the maximum erosion tolerance of vegetation is varied in a range of -2.5 to -2.0 m season^{-1} (the negative sign denotes erosion), whilst the maximum deposition tolerance is varied in a range of 2.9 to 3.2 m season^{-1}. Both ranges are explored with a step resolution of 0.1 m season^{-1} and are part of the spectrum previously explored in Yan & Baas (2017). The sand transport rate is kept at the default of 20 m^3 m^{-1} yr^{-1}. The climatic impact, $I_{climate}$, is varied from -0.10 to -0.46, with a step resolution of 0.02. Multiple simulations are explored to determine a threshold of climatic impact at which the parabolic dune is activated into a barchan. More than 2000 simulations were analysed for this aspect.

2.2.2. Wind strength

The influence of an increase in wind strength on the activation of parabolic dunes is confined to situations in which vegetation is insufficient to entirely prevent sand transport, as a fully vegetated surface cannot be activated purely by an increase in wind strength alone. To examine the influence of increased wind strength on the activation of parabolic dunes, the initial dune is selected at 80, 85, and 90 yrs. of the base simulation of Fig. 1, when the parabolic dune still has a relatively high mobility (*BSF* = 0.34, 0.30, and 0.25, respectively). The maximum erosion and deposition tolerances of the vegetation are varied in a range of -2.5 to -2.0 m season^{-1} and 2.9 to 3.2 m season^{-1} respectively with a step resolution of 0.1 m season^{-1}. The sand transport rate is explored from 110% to 250% of the standard sand transport rate of 20 m^3 m^{-1} yr^{-1} with a step resolution of 10% (i.e. 2 m^3 m^{-1} yr^{-1}), to determine a threshold at which the parabolic dune is transformed into a barchan. A total of 3240 simulation scenarios were analysed for this aspect.

2.2.3. Overgrazing

Severe anthropogenic activity such as overgrazing can activate stabilising parabolic dunes and transform them into highly mobile barchan dunes. For this part of the study all simulation scenarios start from an initial parabolic dune with *BSF* of 0.34 (t_0 = 80 yrs.). The deposition tolerance of vegetation is explored in a range of [2.9, 3.2] m season^{-1}, at a constant erosion tolerance of -2.5 m season^{-1}. On the other hand, to explore the impact of the erosion tolerance on the transformation, the erosion tolerance is then varied in a range of [-2.5, -2.0] m season^{-1}, at a constant deposition tolerance of 3.0 m season^{-1}. The forage demand is varied from 4000 to 6000 units yr^{-1} with steps of 100. This simulated demand can be placed in context of livestock browsing of Ordos Sagebrush: with foliar coverage of this species of roughly 37% (Yang *et al.*, 2008), one shrub (equal to one cell in the model domain) can be thought to provide a maximum forage of 0.37 (in units of vegetation effectiveness). The domain of 400 × 153 m^2, if fully covered in vegetation, can then carry a total of 22644 units of forage. The simulated demand thus represents 18-26% of the total, which is in line with the harvesting coefficients for semi-arid rangelands found by Galt *et al.* (2000). This part of the study involved 189 simulation scenarios in total.

3. Climatic change: reduced water availability

An example in Fig. 2 illustrates a typical dune transformation process from a parabolic dune with *BSF* of 0.34 (t_0 = 80 yrs., Fig. 1) into a barchan under a negative climatic impact. While the arms of the parabolic dune have been fully stabilised by vegetation, the less stabilised lobe in the middle moves forward unimpeded, separating from the parabolic arms and transforming into a barchan dune. As the resulting barchan migrates over the shrub land, continuous incorporation of sand from the substratum and the associated lateral avalanching expands the mobile frontal area and increases the dune size progressively. Under certain conditions, rather than a single barchan a parabolic dune can be activated into multiple barchans or develop into more complicated active parabolic dune forms: elongated, imbricated or digitated. This section shows firstly the resulting dune morphologies under differing reductions in water availability as well as varying mobility of the initial parabolic dune, and secondly analyses parameter controls on the dune transformations. Physical processes and controlling mechanisms are discussed in Section 5.

Transformations of an (originally) stabilising parabolic dune as a consequence of reduced water availability can be classified into four types: elongation of the parabolic dune; a single barchan; multiple barchans; and a barchanoid and/or transverse dunefield (Fig. 3). Simulation scenarios starting with *BSF* of 0.34 (t_0 = 80 yrs.) can only be activated and transformed into a single barchan, occasionally accompanied with much smaller parabolic dunes in the downwind direction. An increase in the climatic impact can eventually lead to the destruction of the original arms of a parabolic dune and the activation of the entire domain, but never yields the development of multiple barchans (type 3 in Fig. 3) as compared with some simulation scenarios with *BSF* of 0.25 (t_0 = 90 yrs.). In this case, as $I_{climate}$ increases from -0.26 to -0.40, the initial parabolic dune transforms from a single barchan into multiple barchans (typically one large barchan following two smaller barchans) (Fig. 4). A stronger climatic impact generally results in a quicker activation of the relatively bare lobe of a parabolic dune, leaving behind shorter arms and developing a larger activation angle. The activation angle is defined as the angle between the two low ridges (parabolic arm remnants) or the edges of the deflation plain which can be derived by linearly fitting two regression lines of both edges (R^2 > 95%). A negative angle denotes the two ridges widening in the downwind direction, and the resulting dune keeps expanding laterally as shown in Fig. 5 (*cf.* Fig. 13 & Appendix D in Yan and Baas, 2017).

Simulation scenarios from the initial parabolic dunes with *BSF* of 0.17 (t_0 = 100 yrs.) and 0.06 (t_0 = 110 yrs.) need a much stronger climatic impact in order to transform into barchans. Both initial parabolic dunes can only be transformed into a barchan with well-preserved remnant parabolic arms at a climatic impact of -0.44. A small further increase of the climatic impact to -0.46 activates the entire domain into a field of barchans with no remnant arms left behind. A large range of weaker climatic impacts, nevertheless encourages the simple parabolic dunes to evolve into more complicated dune morphologies (see Appendix A for a range of examples). Simulations from the initial parabolic dune with *BSF* of 0.00 (t_0 = 120 yrs.) can only be either stabilised completely or be fully activated into a barchan dunefield (no arms). In these situations, the erosion and deposition tolerances of vegetation are irrelevant to determining the threshold of climatic impact to reactivate an initial parabolic dune.

Detailed analysis of the climatic impact threshold on the parabolic-to-barchan dune transformations in the following sections is focused on initial parabolic dunes with *BSF* of 0.34 and 0.25, since starting points with *BSF* below 0.25 require too strong a climatic impact to trigger transformation. The influence of vegetation erosion and deposition tolerances on the threshold of climatic impact is also investigated in detail.

The activation threshold of climatic impact relates closely to the stability of a vegetated parabolic dunefield. As shown in Fig. 6, the *BSF* of the initial parabolic dune strongly controls the activation threshold of climatic impact. As the initial *BSF* decreases from 0.34 (t_0 = 80 yrs.) to 0.25 (t_0 = 90 yrs.), the activation threshold of climatic impact increases significantly. Parabolic dunes at the lower *BSF* require a greater climatic impact to transform into barchans. A high deposition tolerance of vegetation promotes dune stabilisation and requires a relatively greater activation threshold, while the erosion tolerance of vegetation seems to play a minimal role in determining a dune activation threshold.

Fig. 7 shows the relationship between the climatic impact and the activation angle of resulting barchans with *BSF* of 0.34 and 0.25, respectively. As the climatic impact increases, the activation angle becomes more negative. This means that a greater climatic impact results in a more severe lateral expansion and an associated larger size of dunes. The influence of vegetation erosion and deposition tolerances on the activation angle is generally minimal. There is a good linear correlation for both sets of data. Interestingly, the slopes of regression lines are similar, although the larger activation threshold of climatic impact for parabolic dunes with *BSF* of 0.25 limits the data set into a smaller range. This correlation between the climatic impact and the activation angle seems independent of the stability of the initial parabolic dunes, and may be potentially used to estimate the severity of a climatic impact based on field measurements of activation angles. A large activation angle also means that the dune is more easily merged with any neighbouring dunes, which may result in the development of transverse dunes.

As the climatic impact increases on a transforming dune with an initial *BSF* of 0.34, the *transition time*, defined as the time when the transforming dune starts to exhibit a barchan shape with a crescentic lobe and clearly identifiable toe and slip faces, decreases first and then levels off at a duration of roughly 40 yrs beyond a climatic impact of -0.26 (Fig.8). The transition time only decreases further at very severe climatic impacts, but this is close to the point where the entire domain transforms into a bare-sand dunefield (as in Fig. 3 example iv). For a dune transformation starting from *BSF* = 0.25, the transition time steadily decreases as climatic impact grows, until a minimum duration, again, of roughly 40 yrs. Comparison between the two scenarios of Fig. 8 shows that more stabilised initial parabolic dunes require a longer time to be transformed into barchans, and the transition time increases more significantly for a relatively small climatic impact. An increase in the deposition tolerance of vegetation discourages the activation of parabolic dunes and hence leads to longer transition duration. This control becomes stronger as the climatic impact is less severe. The effect of erosion tolerance of vegetation on the transition time does not show any particular trend or pattern.

Fig. 9 shows the relationship between the activation angle and the dune surface erodibility at the transition time. A larger activation angle is generally associated with a higher dune surface erodibility at the transition time. It suggests that the correlation may be independent of the degree of stability of an initial parabolic dune, although a more stabilised initial parabolic dune results in a wider distribution and a higher randomness. The influence of the erosion and the deposition tolerances does not show a clear trend.

4. Climatic change: increased wind strength

The vegetation cover and the associated stability of an initial parabolic dune strongly control the activation threshold of sand transport rate (Fig. 10). A higher deposition tolerance of vegetation increases the activation threshold of sand transport rate, although the influence of the erosion tolerance of vegetation seems minimal.

The activation angle generally increases with the sand transport rate, although there is no outstanding trend with respect to the erosion and the deposition tolerances of vegetation (Fig. 11). Although the activation threshold of sand transport rate varies for different initial parabolic dunes, the average activation angles under the same sand transport rate are similar and seem independent of the stability of the initial parabolic dunes. The slopes of regression lines derived from different initial parabolic dunes vary within a magnitude of 0.1. As a consequence, by comparing activation angles of different mobile dunes, it is potentially possible to deduce the associated sand transport regimes: larger activation angles imply a wind regime with higher sand transport rates.

As the sand transport rate increases, the transition time of parabolic dunes into barchans decreases, as shown in Fig. 12. The degree to which an increase in the sand transport rate reduces the transition time, however, dwindles rapidly. The transformation is hence only sensitive to changes in sand transport rate close to the activation threshold. Further increases in sand transport rate do not significantly contribute to a quicker activation of parabolic dunes. Given the same sand transport rate, a more stabilised parabolic dune requires a longer transition time. The erosion and the deposition tolerances only exert limited impacts on the transition time when the sand transport rate is relatively small, just above the activation threshold. A higher erosion tolerance of vegetation encourages a quicker barchan-to-parabolic dune transformation, whereas a higher deposition tolerance of vegetation prolongs the transition duration.

5. Processes and mechanisms of the parabolic-to-barchan dune transformation

A barchan-to-parabolic dune transformation under climatic change can be conceptualised into stages illustrated by snapshots in Fig. 13. The negative climatic impact reduces the capability of vegetation to withstand erosion and sand burial. More severe erosion causes vegetation on the inner slope of the arms close to the edges of the lobe to decline (*Zone i* outlined by Δbcd at t_0 in Fig. 13). The decline of vegetation in *Zone i* enables sand there to be transported and deposited onto *Zone ii* outlined by Δabc. As the lobe migrates forward, the *Zone ii* ends up on the windward slope and undergoes erosion (*Line ab* at t = +21 yrs. in Fig. 13). Beyond *Line ac* in

Zone iii, vegetation is able to withstand the climatic impact and neither erosion nor deposition occurs. The *Zone iii*, therefore, develops to be part of the trailing arm.

The erosion on the inside of the trailing arms provides more sand for transport and deposition on the lee slope downwind, thereby exerting a more severe negative impact on the vegetation there. More severe decline of vegetation on the edges of the lobe, meanwhile, further accelerates migration thereof as compared with the lobe in the middle. This is due to the fact that: (1) the vegetated area on the lower slope can maintain a steeper gradient than the bare surface on the upper slope, and the more severe decline of vegetation close to the lobe edges yields more abundant sand for advancing downwind (Fig. 14); (2) a lower height on the lobe edges can lead to a faster migration rate (provided that the potential sand transport rate is the same), which encourages the formation of a more rounded frontal edge of the dune lobe.

As *Line ab* (t_0 in Fig. 13) first experiences stronger deposition, more severe erosion occurs when *Line ab* subsequently becomes part of the windward slope as the lobe migrates forward (t = +21 yrs. in Fig. 13). This is when a catastrophic shift begins. From that time onwards, severe erosion takes place on the vegetated edges of the lobe and the lobe is gradually separating from the trailing arms. The severe erosion provides more and more abundant sediment supply for sand transport from vegetated lobe edges along with incorporating sand from the sandy substratum underneath. This reinforces the vegetation decline on the lee slope and a faster migration rate on the lobe edges (because of a lower height). As a result, the maximum height that vegetation can reach on the lee slope decreases (see *Point e* and *Point f* at t = +30 yrs. in Fig. 13).

On the one hand, a faster migration of the lobe edges and lateral avalanching expand the frontal area, and vegetated edges of the lobe decrease in height because of vegetation decline arising from climatic impact; on the other hand, the vegetated edges that have already survived sand burial can only be eliminated by erosion because no sand supply is available upwind (since the activation angle is negative). As a result, an incipient crescentic ridge forms due to a faster migration rate on the edges as compared with the main body in the middle. At the same time, the centre of the parabolic ridge is maintained because of the greater height where vegetation had survived sand burial before the catastrophic shift occurred (see the *Point e* in Fig. 13). Continued erosion of vegetated edges lowers the height of the parabolic ridge due to the decrease in the maximum height vegetation can survive on the lee slope (see *Point f* in Fig. 13). The parabolic ridge eventually disappears when the vegetated lobe edges are no longer higher than the newly-created low ridge of the resulting barchan with a typical slip face (t = +67 yrs. in Fig. 13).

The initial parabolic dune transforms into a single barchan when the migration rate of the lobe edges is similar to the erosion rate of previously better-vegetated edges (or the parabolic ridge), as in the example described above. However, if the migration rate of the lobe edges is much faster than the erosion rate of the parabolic ridge, for a relatively large dune, for instance, multiple barchans can develop (Fig. 4b). The lower erosion rate of the parabolic ridge slows down the migration of the central body, whereas the faster migration rate of lobe edges results in the escape of sand from the main body and the formation of smaller sand piles downwind (where severely deteriorated vegetation on the interdune areas is incapable of preventing fast migration). The continuous escape of sand from the main body and the accumulation of these piles can further lead to the development of barchans. The main body eventually transforms into a larger barchan as soon as the parabolic ridge has been completely eroded.

A severe climatic change arising from reduced water availability or increased wind energy can lead to the development of a larger activation angle, because (1) more severe vegetation decline on the lobe edges leads to more extensive lateral avalanching and a faster expansion of the frontal areas (the lee slope), and (2) the *Point e* is at a lower height and the catastrophic shift happens more quickly, which also leaves behind shorter remnants of the parabolic trailing arms. The activation angle seems independent of the stability of the initial parabolic dunes, indicating that although *BSF* of the initial parabolic dune impacts the threshold of required climatic change, the magnitude of climatic change controls the degree of activation of parabolic dunes once the dune activation processes have been initiated.

A higher deposition tolerance reduces the difference in migration rate on the lobe edges in comparison with the central body, thereby prolonging the transition duration of the parabolic-to-barchan dune transformation. The erosion tolerance of vegetation does not seem to impact the transformation significantly, but likely affects the pattern of resulting barchans (single vs. multiple barchans) because of the effect on the erosion rate of the parabolic ridge. The characteristics of vegetation only play a significant role at a smaller climatic change. This suggests that the influence of severe climatic change on the dune transformation is largely independent from the flora in different regions.

6. Anthropogenic pressure: overgrazing

Grazing activity has a major impact on partially vegetated dunefields, as on the Ordos Plateau, due to their great vulnerability to environmental changes. Fig. 15

exemplifies how grazing activity can lead to an initial parabolic dune being transformed into a highly mobile barchan. The general processes involved are similar to that of the parabolic-to-barchan dune transformations arising from reduced water availability or increased wind energy. The greater impact of vegetation decline on the lobe edges, as compared with the central body, results in a faster migration there, because of the gentler angle of repose for bare surfaces as well as the lower crest of the longitudinal profile. As sand is continuously incorporated into the migrating lobe from the sandy substratum and the eroded arms, the mobile lobe grows in size and expands laterally, transforming into a barchan eventually. In contrast to natural environmental changes which affect relatively weak and young plants more, anthropogenic forces including grazing activity can exert a broad impact on all plants regardless of size or age. As a result, well-vegetated interdune areas have also been activated slightly, leading to the development of low relief.

With increasing forage demand, the transition time of the parabolic-to-barchan dune transformation decreases at a lower rate (Fig. 16a). A small increase in forage demand just above the activation threshold therefore has the most significant impact on transition time. Fig. 16b and c show respectively the influence of the deposition tolerance and the erosion tolerance of vegetation on the forage demand threshold - the minimum forage demand that leads to the parabolic-to-barchan dune transformation. A higher deposition tolerance enables a dune system to withstand a larger forage demand before the dune stabilising processes are reversed, whereas the erosion tolerance seems to play a less direct role in determining the threshold of the parabolic-to-barchan dune transformation.

7. Discussion

Projections of more frequent drought in various regions may indicate more severe dune activations in the future (IPCC, 2013), an example of which has been observed at the Great Sand Dunes in Colorado (Marín *et al.*, 2005). The modelling results highlight that the relationship between erodibility and erosivity is susceptible to climatic changes (Thomas *et al.*, 2005). Although for different reasons, the processes involved in the parabolic-to-barchan dune transformations are much alike. The modelling results shed important light on the eco-geomorphic interactions governing the transformations.

7.1. Eco-geomorphic interaction zones

The importance of eco-geomorphic interactions and the associated morpho-dynamics in controlling barchan-to-parabolic dune transformations has been examined and discussed in detail by Yan and Baas (2017). These eco-geomorphic interaction zones bear different functionality in the processes of dune transformations, and have distinctive characteristics in terms of the balance between sand transport versus vegetation dynamics that can be linked to the consequent topographic development and used to signify the stability of a dune system. In a similar manner, the characteristics of eco-geomorphic interactions during the mobilisation of a parabolic back into a barchan dune also exhibit distinctive behaviours in different areas of the changing dune body. We can identify four basic eco-geomorphic interaction zones that bear different functionality in the transformation of a parabolic into a barchan dune. These zones are illustrated along transverse sections at two stages along the transformation, corresponding to transects at two different spatial locations in the model domain (as the transforming dune is migrating eastward). The first transverse section, at 250 m eastings (Fig. 17), represents a typical example showing how eco-geomorphic interaction zones respond to climatic change during the initial stage of the parabolic-to-barchan dune transformation when the transforming dune still maintains a parabolic shape. The second transverse section, at 325 m eastings (Fig. 19), demonstrates typical eco-geomorphic interaction zones when the parabolic dune has transformed into a typical barchan dune with a slip face.

Fig. 17 shows an example of how vegetation interacts with a migrating parabolic dune under climatic impact during the initial stage, and Fig. 19 presents the temporal changes in height and vegetation effectiveness in four basic eco-geomorphic interaction zones, going from the outer edge to the dune centre-line. It can be seen that Zone 1, which develops into the outside slope of the arms, is almost eliminated (Fig. 17). Zone 2, which develops into the inner slope of the arms, is very thin due to severe impact of erosion (Fig. 18b) and as a result, trailing arms are no longer left behind. Vegetation in Zone 3 declines slightly first due to sand burial, and then is eliminated by more severe erosion (Fig. 18c). Zone 4, the maximum height where vegetation can survive remains constant (Fig. 18d). In comparison to the barchan-to-parabolic dune transformation (Yan and Baas, 2017), Zone 1 and Zone 2 of the initial parabolic dune - the only areas where vegetation is able to trap sand and stabilise the dune - are squeezed significantly under climatic impact. Consequently, the lobe expands in size due to the continuous incorporation of sand from its substratum underneath, and with only minimal loss of sand to trailing arms.

After the initial stage above, eco-geomorphic-interaction zones when the parabolic dune has completed the transformation into a barchan are presented in

Fig. 19 and Fig. 20. The characteristics of Zone 1 and Zone 2 are similar to their counterparts in the initial stage of the parabolic-to-barchan dune transformation under climatic impact in Fig. 18. No outstanding arm is developed and the ridge is only 2 m in height (Fig 20a & b). Vegetation in Zone 2 declines slightly first because of sand burial and dies eventually because of erosion. The characteristics of Zone 3 are different from the counterparts of the initial stage of the parabolic-to-barchan dune transformation (Fig. 18c). Vegetation in the Zone 3 can survive similar sand deposition and dies of further sand burial (Fig. 20c). The *Point c* is the front most of the barchan horn as migrating dune cross the transverse section (t = +55 yrs. in Fig. 19a), but it is the last to be eroded out of the deflation plain (t = +90 yrs. in Fig. 19). This indicates that the barchan dune is interacting with vegetation and expanding laterally. The Zone 4 comprises the transverse section of the crescentic-shaped body in the centre of the dune, and the changes in both topography and vegetation display a similar profile (Fig. 20d).

7.2. **Implications**

As discussed above for both stages, the characteristics of four eco-geomorphic interaction zones closely relate to the processes of dune transformations, and may be potentially used to predict dune stability under climatic change in a real dunefield. Comparing modelling results herein against real-world data, however, requires further research. The modelling results suggest that the mobility of an initial parabolic dune at the outset of perturbations determines to a large extent the capacity of a system to absorb the environmental change and the propensity for activation and dune transformation. A slight increase in vegetation cover of an initial parabolic dune can increase the activation threshold of climatic impact (both drought stress and wind strength) significantly, consistent with findings suggested by Nield and Baas (2008) that dune systems may exhibit a strong threshold response. Wiggs *et al.* (1995) have also found that an increase in water stress or wind strength can impair vegetation cover and a sparse vegetation cover raises the potential for surface mobility. A model proposed by Yizhaq *et al.* (2007) indicates a similar behaviour that sufficiently high wind power can cause the decay of vegetation and activate stabilised dunes, and that changes in windiness and vegetation cover may shift the dune into a new state (Barchyn and Hugenholtz, 2013; Yizhaq *et al.*, 2009). The modelling results suggest that there is positive feedback between the decline of vegetation and the increase of sand availability (Brunsden and Thornes, 1979). A higher vegetation cover of initial parabolic dunes can dampen out small perturbations and enables the system to maintain the existing state (Hugenholtz and Wolfe, 2005).

The modelling results show that the characteristics of vegetation play a less important role in the dune activation and parabolic-to-barchan dune transformations, as compared with the dune stabilisation investigated in Yan and Baas (2017). A higher deposition tolerance can increase the activation threshold of both climatic impact and sand transport rate slightly, but the influence of vegetation characteristics becomes negligible when the mobility of an initial parabolic dune is very low. As an extreme example, simulations from the initial parabolic dune at 120 yr can only be *either* fully stabilised *or* fully activated into a bare-sand dunefield by climatic impact, resembling findings by Nield and Baas (2008). A highly vegetated parabolic dune cannot easily be activated and transformed into a barchan dune; instead, it results in more diverse dune morphologies and develops into a more complicated imbricated or nested parabolic dune, as shown in Appendix A. This seems to suggest that there is correlation between the complexity of dune morphology and the stability of the initial parabolic dunes. A long-term drought can, however, deplete vegetation and can reactive a dune significantly (Mangan *et al.*, 2004). In contrast, stabilised parabolic dunes cannot be activated by increasing sand transport rate without catastrophic events such as fires or storms, because no sand is available for mobilisation. This indicates that under limited sand supply drought severity exerts more severe impacts on dune activation than windiness.

Beyond the threshold of a parabolic-to-barchan dune transformation, a small increase in either climatic impact or sand transport rate can accelerate the dune activation and transformation significantly, while a larger increase has a progressively decreasing effect. A low erosion or deposition tolerance leads to the development of resulting barchan dunes with a higher dune surface erodibility. The influence of vegetation characteristics is more outstanding for an initial parabolic dune with higher stability. The different sensitivity caused by varying initial dune stability become less significant as the climatic impact increases, but does not show apparent change as the sand transport potential increases. This may be due to the fact that there is no significant difference in terms of sand availability even though vegetation cover is slightly different. As a result, vegetation characteristics play a less important role because of the limitation by sand availability even when sand transport potential increases substantially.

The modelling results also show that the characteristics of eco-geomorphic interaction zones involved in the dune activation are significantly different from that of dune stabilisation studied in Yan and Baas (2017). Therefore, the change in the characteristics of eco-geomorphic interaction zones may indirectly reflect and predict the direction of an ongoing transformation. The activation angle is another interesting feature. There is a strong linear correlation between the climatic impact or the sand transport rate and the activation angle, independent of the stability of the initial parabolic dune and the activation threshold. The activation angle, therefore, may be potentially measured in the field from the remnants of parabolic arms left behind, and used as a proxy of the environmental stresses that lead to the transformation. In the context of a whole dunefield being affected, however, any remnant parabolic arms may be quickly erased as neighbouring and upwind dune transformations override the relic topography. Similarly, in cases of a large activation angles (corresponding to large climatic impacts) a transforming dune more easily merges neighbouring dunes, which may result in the emergence of transverse ridges.

The response of dune morphology to environmental changes often involves time-lags. The modelling results suggest a reaction time of approximately 5 years before a dune starts to change its morphology in response to climatic change. Vegetation acts as a buffer between environmental changes and morphological responses, a prevalent phenomenon that has been observed in many studies. Lancaster and Helm (2000) have found that a lag between changes in precipitation and vegetation makes the dune mobility index incompetent to predict a short-term change in sand transport. Mangan *et al.* (2004) have contributed dunes at the High Plains remaining stable during the 1930s drought to the presence of plant rooting systems that can bind soil for a period of time even though the plants have died of drought. Hesse and Simpson (2006) found perennial plant cover predominantly controls the mobility of dunes in Australia. They also observed that the perennials have a response time longer than the inter-annual variations of precipitation, and seem to respond to cyclical droughts on a temporal scale of years to decades before impacting sand transport patterns over dunes. Compared with the response of dune morphology to environmental changes, vegetation is more sensitive and can thus be potentially used as an indicator for predicting the activation of vegetated parabolic dunes. In particular, the decline of vegetation on the lee slope and the windward slope close to the dune lobe is likely to be the first sign of dune activation and the subsequent parabolic-to-barchan dune transformation.

Our previous study on barchan stabilisation under ameliorating vegetation conditions showed that larger barchans can be more easily and more quickly stabilised and transformed into parabolic dunes due to their lower migration rates (Yan and Baas, 2017). When negative stresses (either from climate change or human disturbance) are then imposed on a field of stabilising parabolic dunes of varying sizes, the stabilisation processes are reversed on lobes with varying degrees of Bare Surface Fraction, and these different parabolic dunes will hence respond in different manners, as shown in the results above. Parabolic dunes with a high *BSF* may be activated and transformed into barchans, whereas parabolic dunes with a relatively low *BSF* develop from simple forms into more complicated forms. The spatial arrangements and the history of individual dunes, therefore, play an important role in shaping the spatial heterogeneity of a dunefield. This may be an important reason why highly mobile barchans have been found to coexist with well-vegetated parabolic dunes in the field, such as dunefields in north-eastern Brazil (Yizhaq *et al.*, 2007). In a related context, Tsoar (2005) and Yizhaq *et al.* (2009) have established the hysteresis behaviour of activation versus stabilisation of dunefields, showing that dormant dunefields that have been activated due to an increased environmental forcing require a decrease in that forcing far below its initial level in order to restore the dunefield to its original dormant state. Our results illustrate a similar behaviour in that it is exceedingly difficult for initially highly vegetated parabolic dunes to restore to this original state once they have been mobilised into barchans.

8. Conclusions

The activation of vegetated parabolic dunes into highly mobile barchans poses a threat to both ecological sustainability and social-economic development. The Extended-DECAL has been used to explore the sensitivity of parabolic dunes on environmental changes arising from the increases in drought stress, wind strength, and grazing activities, informed by field measurements and remote sensing interpretations. The model has been able to simulate the activation of vegetated parabolic dunes into barchans on plausible temporal scales (several decades to 100 years) and spatial scales (tens to hundreds of meters). It shows that the deposition tolerance of vegetation significantly influences the transition time and the resulting dune morphology. A higher deposition tolerance enables vegetation downwind of a partially vegetated parabolic dune to resist stronger climatic impact, and hence results in gentler activation and a longer transition time into a barchan. In contrast, the erosion tolerance of vegetation plays a less significant role in controlling the rate of dune transformations, but it is essential to the development of trailing arms of parabolic dunes and influences the lateral expansion of an activated dune lobe into a highly mobile barchan.

Sand availability in a closed environment is primarily controlled by the size of dunes and the thickness of sandy substratum underneath. A high sand availability arising from larger surface erodibility of an initial parabolic dune increases sand transport and requires a smaller climatic impact to be activated into a barchan, because sand availability, instead of wind energy, is the limiting factor for sand transport in such an environment where dunes are surrounded by a well-vegetated interdune plain. An increase in potential sand transport rate accelerates the dune migration, thereby shortening the transition time of the parabolic-to-barchan dune transformation. The activation angle is closely related with the rate of dune activation and may provide a useful linkage between field measurements and numerical predictions. The characteristics of eco-geomorphic interaction zones are more sensitive to environmental changes as compared with dune morphologies, and can be potentially used as a proxy to identify and monitor the stability of a vegetated dune system. The modelling results indicate that the grazing activity, in comparison with climatic impact, can more easily result in dune activation and the transformation from vegetated parabolic dunes into barchan dunes.

The model can be easily adapted to a different dune environment, and be used to explore various scenarios under changes in both natural and anthropogenic controls. A relatively low computational demand enables extensive explorations of phase space and phase diagrams, detailed investigations of complicated interactions between relatively large numbers of system parameters, which can then assist in understanding various eco-geomorphic processes of a dune system in a more integrated manner.

Acknowledgements

We greatly appreciate the detailed and constructive comments from three anonymous reviewers as well as the editors, which have led to, we hope, an improved manuscript with greater clarity and robustness. This research was supported by the Graduate School at King’s College London, a postgraduate research grant from British Society for Geomorphology, a Dudley Stamp Memorial

Award from the Royal Geographical Society, and the National Natural Science Foundation of China (40171002, 41402125).

References

Anton, D., Vincent, P., 1986. Parabolic dunes of the Jafurah Desert, Eastern Province, Saudi Arabia. Journal of Arid Environments, 11(3), 187-198.

Arens SM, Slings Q, de Vries CN. 2004. Mobility of a remobilised parabolic dune in Kennemerland, The Netherlands. Geomorphology 59: 175-188.

Barchyn, T.E., Hugenholtz, C.H., 2013. Reactivation of supply-limited dune fields from blowouts: A conceptual framework for state characterization. Geomorphology, 201(0), 172-182.

Brunsden, D., Thornes, J.B., 1979. Landscape Sensitivity and Change. Transactions of the Institute of British Geographers, 4(4), 463-484.

Carter, R.W.G., Hesp, P.A., Nordstrom, K.F., 1990. Erosional landforms in coastal dunes. In: K.F. Nordstrom, N.P. Psuty, R.W.G. Carter (Eds.), Coastal Dunes: Form and Process. John Wiley & Sons Ltd., Chichester.

Galt D, Molinar F, Navarro J, Joseph J, Holechek J. 2000. Grazing capacity and stocking rate. Rangelands: 7-11.

Goudie A. 2011. Parabolic Dunes: Distribution, Form, Morphology and Change. Annals of Arid Zone 50: 1-7.

Hesp, P., Martinez, M., da Silva, G.M., Rodriguez-Revelo, N., Gutierrez, E., Humanes, A., Lainez, D., Montano, I., Palacios, V., Quesada, A., Storero, L., Trilla, G.G., Trochine, C., 2011. Transgressive dunefield landforms and vegetation associations, Dona Juana, Veracruz, Mexico. Earth Surface Processes and Landforms, 36(3), 285-295.

Hesp, P.A., 2001. The Manawatu Dunefield: Environmental Change and Human Impacts. New Zealand Geographer, 57(2), 33-40.

Hesse, P.P., Simpson, R.L., 2006. Variable vegetation cover and episodic sand movement on longitudinal desert sand dunes. Geomorphology, 81(3-4), 276-291.

Hugenholtz, C.H., Wolfe, S.A., 2005. Biogeomorphic model of dunefield activation and stabilization on the northern Great Plains. Geomorphology, 70(1-2), 53-70.

IPCC, 2013. Climate change 2013: the physical science basis. Contribution of working group I to the fifth assessment report of the intergovernmental panel on climate change. Cambridge University Press, New York.

Jiang, H., Zhang, P.Y., Zheng, D., Wang, F.H., 1995. The Ordos Plateau of China. In: J.X. Kasperson, R.E. Kasperson, B.L. Turner II (Eds.), Regions at risk: comparisons of threatened environments. The United Nations University, Tokyo.

Kobayashi, T., Liao R.T., Li S.Q., 1995. Ecophysiological behavior ofArtemisia ordosica on the process of sand dune fixation. Ecological Research 10: 339-349.

Lancaster, N., Helm, P., 2000. A test of a climatic index of dune mobility using measurements from the southwestern United States. Earth Surface Processes and Landforms, 25(2), 197-207.

Mangan, J., Overpeck, J., Webb, R., Wessman, C., Goetz, A.H., 2004. Response of Nebraska Sand Hills Natural Vegetation to Drought, Fire, Grazing, and Plant Functional Type Shifts as Simulated by the Century Model. Climatic Change, 63(1-2), 49-90.

Marín, L., Forman, S.L., Valdez, A., Bunch, F., 2005. Twentieth century dune migration at the Great Sand Dunes National Park and Preserve, Colorado, relation to drought variability. Geomorphology, 70(1–2), 163-183.

McKee, E.D., 1966. Structures of dunes at white sands national monument, New Mexico. Sedimentology, 7(1), 3-69.

Muckersie, C., Shepherd, M.J., 1995. Dune phases as time-transgressive phenomena, Manawatu, New Zealand. Quaternary International, 26, 61-67.

Nield, J.M., Baas, A.C.W., 2008. The influence of different environmental and climatic conditions on vegetated aeolian dune landscape development and response. Global and Planetary Change, 64(1–2), 76-92.

Pye K. 1982. Morphological development of coastal dunes in a humid tropical environment, Cape Bedford and Cape Flattery, North Queensland. Geografiska Annaler Series a-Physical Geography 64: 213-227.

Pye, K., Tsoar, H., 1990. Aeolian sand and sand dunes. Unwin Hyman Ltd, London.

Ravi, S., Breshears, D.D., Huxman, T.E., D'Odorico, P., 2010. Land degradation in drylands: Interactions among hydrologic–aeolian erosion and vegetation dynamics. Geomorphology, 116(3–4), 236-245.

Rubin, D.M., Hunter, R.E., 1987. Bedform alignment in directionally varying flows. Science, 237(4812), 276-278.

Shulmeister, J., Lees, B.G., 1992. Morphology and chronostratigraphy of a coastal dunefield; Groote Eylandt, northern Australia. Geomorphology, 5(6), 521-534.

Stetler, L.D., Gaylord, D.R., 1996. Evaluating eolian-climatic interactions using a regional climate model from Hanford, Washington (USA). Geomorphology, 17(1–3), 99-113.

Story R. 1982. Notes on parabolic dunes, winds and vegetation in Northern Australia. CSIRO Australian Division of Water and Land Resources 43: 1-33.

Thomas, D.S.G., Knight, M., Wiggs, G.F.S., 2005. Remobilization of southern African desert dune systems by twenty-first century global warming. Nature, 435(7046), 1218-1221.

Tsoar, H., 2005. Sand dunes mobility and stability in relation to climate. Physica A, 357(1), 50-56.

Tsoar, H., Blumberg, D.G., 2002. Formation of parabolic dunes from barchan and transverse dunes along Israel's Mediterranean coast. Earth Surface Processes and Landforms, 27(11), 1147-1161.

Wasson, R.J., Hyde, R., 1983. Factors determining desert dune type. Nature, 304(5924), 337-339.

Werner, B.T., 1995. Eolian dunes: Computer simulations and attractor interpretation. Geology 23: 1107-1110.

Werner, B.T., 1999. Complexity in Natural Landform Patterns. Science 284: 102-104.

Wiggs, G.F.S., Thomas, D.S.G., Bullard, J.E., Livingstone, I., 1995. Dune mobility and vegetation cover in the Southwest Kalahari desert. Earth Surface Processes and Landforms, 20(6), 515-529.

Yan, N., Baas, A.C.W., 2015. Parabolic dunes and their transformations under environmental and climatic changes: Towards a conceptual framework for understanding and prediction. Global and Planetary Change, 124(0), 123-148.

Yan N, Baas ACW. 2017. Environmental controls, morphodynamic processes, and ecogeomorphic interactions of barchan to parabolic dune transformations. Geomorphology 278: 209-237.

Yan N, Hasi E, Liu, H.Q., Li S.Q., 2010. Research progress in morphology and evolution of the parabolic dunes. Journal of Desert Research 30: 801-807.

Yang H, Zhange J, Li Z, Wu B, Zhang Z, Wang Y., 2008. Comparative study on spatial patterns of Artemisia ordosica populations in the Mu Us sandy land. Acta Ecologica Sinica 28: 1901-1910.

Yizhaq, H., Ashkenazy, Y., Tsoar, H., 2007. Why Do Active and Stabilized Dunes Coexist under the Same Climatic Conditions? Physical Review Letters, 98(18), 188001.

Yizhaq, H., Ashkenazy, Y., Tsoar, H., 2009. Sand dune dynamics and climate change: A modeling approach. Journal of Geophysical Research: Earth Surface, 114(F1), F01023.

Zheng, Y., Xie, Z., Jiang, L., Shimizu, H., Rimmington, G.M., Zhou, G., 2006. Vegetation responses along environmental gradients on the Ordos plateau, China. Ecological Research, 21(3), 396-404.

Fig. 1. Base simulation from Yan and Baas (2017) of a migrating barchan dune transforming into a parabolic dune under the influence of stabilising vegetation (above), used for selecting starting points for initiating re-mobilising impacts (below). The simulation starts from an initial 9.2 m high barchan on a 0.6 m thick sandy substratum, affected by vegetation with a maximum erosion tolerance ($\tau_{E\_physioMax}$) of -2.3 m season^{-1} and a maximum deposition tolerance ($\tau_{D\_physioMax}$) of 3.0 m season^{-1}. (a) Topography shown in shaded 3D in upper sequence (white deflation plain indicating exposed non-erodible base of the modelling domain), with lower sequence showing vegetation effectiveness (ρ), superimposed on the shaded topography. Vegetation on the surrounding plain is masked out, so that parabolic arms and frontal edge of dune can be clearly identified. See vertical colour bar on the right for different degrees of vegetation effectiveness. (b) Changes in Bare Surface Fraction (*BSF*) during the base simulation. The green dot denotes the moment when the initial barchan is transformed into a typical parabolic dune. Pink asterisks and orange triangles denote initiation times when decreased water availability or increased wind strength is imposed onto the system, respectively.

Fig. 2. An example of the parabolic-to-barchan dune transformation triggered by environmental change. The initial state (t_0) is the parabolic dune at 80 yrs. in Fig.1 (*BSF* = 0.34), and a climatic impact ($I_{climatic}$) of -0.14 was imposed onto the vegetation, analogous to a drought situation. Simulation parameters: q = 20 m^3 m^{-1} yr^{-1}, $\tau_{E\_physioMax}$ = -2.3 m season^{-1}, and $\tau_{D\_physioMax}$ = 3.0 m season^{-1}. Shaded topography, left, and overlain with maps of vegetation effectiveness, right, (colour bar legend on bottom right) as described in Fig.1. An example is also presented in Video 1 and Video 2 [supplemental].

Fig. 3. Resulting dune morphologies (indicative topography only) from a parabolic dune with an initial *BSF* = 0.25 (t_0 = 90 yrs.) under climatic impacts. Vegetation parameters: $\tau_{E\_physioMax}$ = -2.0 m season^{-1}, and $\tau_{D\_physioMax}$ = 2.9 m season^{-1}. $I_{climatic}$ increases from -0.22, -0.28, -0.32, to -0.46 in this sequence from bottom to top. (i) The parabolic dune continues to be stabilised and its lobe hardly changes in shape. (ii) The lobe of the parabolic dune is mobilised and separates from the trailing arms to develop into a single barchan, whilst the remnant arms remain intact. (iii) The lobe of the parabolic dune transforms into multiple barchans, whilst the trailing arms remain intact. (iv) The whole domain is activated, and the trailing arms of the parabolic dune are destroyed.

Fig. 4. Transformation of a parabolic dune with an initial *BSF* = 0.25 (t_0 = 90 yrs.) into: (a) a single barchan, $I_{climate}$ = -0.26 vs. (b) multiple barchans, $I_{climate}$ = -0.40. Simulation parameters: q = 20 m^3 m^{-1} yr^{-1}, D_0 = 0.6 m, $\tau_{E\_physioMax}$ = -2.1 m season^{-1}, and $\tau_{D\_physioMax}$ = 2.9 m season^{-1}. An example is also presented in Video 3 [supplemental].

Fig. 5. An example of the activation angle (β) in a simulation.

Fig. 6. Influence of the maximum erosion tolerance ($\tau_{E\_physioMax}$; see legend) and the maximum deposition tolerance ($\tau_{D\_physioMax}$; horizontal axis) of vegetation on the activation threshold for the climatic impact.

Fig. 7. Influence of the climatic impact ($I_{climate}$; horizontal axis) on the activation angle (β; vertical axis), under a range of vegetation characteristics. Crosses denote means of simulations with different maximum erosion tolerance ($\tau_{E\_physioMax}$) and maximum deposition tolerance ($\tau_{D\_physioMax}$), and whiskers denote standard deviations. Lines show linear regressions with dashed contours indicating 95% confidence intervals.

Fig. 8. Influence of the climatic impact ($I_{climate}$) and the characteristics of vegetation on the dune transition time (t_{tran}). Colours labelled in the legend denote the relevant vegetation characteristics, while crosses and whiskers denote means and standard deviations over the range of simulations.

Fig. 9. The relationship between the activation angle (β) and Bare Surface Fraction (*BSF*) at the transition time (t_{tran}). Blue circles and red triangles denote simulations from parabolic dunes at initial *BSF* of 0.34 and 0.25, respectively. The black line denotes the best-fit linear regression line through all points, with blue contour lines indicating 95% confidence intervals.

Fig. 10. Influence of the maximum erosion tolerance ($\tau_{E\_physioMax}$) and the maximum deposition tolerance ($\tau_{D\_physioMax}$) of vegetation on the activation threshold of sand transport rate (q). Initial parabolic dunes have different degrees of bare surface fraction (*BSF*).

Fig. 11. The relationship between sand transport rate (q) and activation angle (β). (a) Simulations from three different initial BSF states (see legend) shown separately, crosses and whiskers indicating means and standard deviations over the range of

vegetation characteristics. Best-fit linear regressions shown with colours matching the legend. (b) Single linear regression through all means shown in (a) combined, with dotted contours indicating 95% confidence intervals.

Fig. 12. The relationship between the sand transport rate (q) and the transformation time (t_{tran}) under influence of the different maximum erosion tolerance ($\tau_{E\_physioMax}$) and the maximum deposition tolerance ($\tau_{D\_physioMax}$). Colours labelled in the legend denote the erosion or deposition tolerances, while crosses and whiskers denote means and standard deviations of the range of $\tau_{E\_physioMax}$ or $\tau_{D\_physioMax}$.

Fig. 13. Snapshots showing stages of the parabolic-to-barchan dune transformation. Colour maps of vegetation effectiveness (ρ; see colour scale bar bottom right) superimposed on shaded topography. Simulation parameters: initial BSF = 0.34 (t_0 = 80 yrs.), q = 20 m^3 m^{-1} yr^{-1}, $\tau_{E\_physioMax}$ = -2.1 m season^{-1}, $\tau_{D\_physioMax}$ = 2.9 m season^{-1}, and $I_{climate}$ = -0.14. The purple dashed square in bottom panel indicates the zoomed-in area of the upper panels.

Fig. 14. Different migration rates arising from the different maximum height where vegetation exists on the lee slope. Vegetation initially colonises a higher vertical position on the lee slope of profile (a) than of profile (b) at time t_1. When vegetation declines to a similar position in height at t_2, the avalanching of sand on the upper slope of profile (a) is more severe than that of profile (b), because the vegetated area maintained a steeper slope than the bare surface. This then results in a further and faster migration of profile (a) as compared with profile (b).

Fig. 15. An example of the parabolic-to-barchan dune transformation arising from grazing activity. Colour maps of vegetation effectiveness (ρ; see colour scale bar bottom panel) superimposed on shaded topography. Simulation parameters: initial $BSF = 0.34$ ($t_0 = 80$ yrs.), $q = 20$ m^3 m^{-1} yr^{-1}, $\tau_{E\_physioMax} = -2.5$ m season^{-1}, and $\tau_{D\_physioMax} = 3.0$ m season^{-1}. The imposed foraging demand is 0.080 m^{-2} yr^{-1}. An example is also presented in Video 4 [supplemental].

Fig. 16. Impact of grazing on the parabolic-to-barchan dune transformation. (a) Relationship between foraging demand and transition time (t_{tran}). Simulation parameters: initial $BSF = 0.34$ ($t_0 = 80$ yrs.), $q = 20$ m^3 m^{-1} yr^{-1}, $\tau_{E\_physioMax} = -2.5$ m season^{-1}, and $\tau_{D\_physioMax} = 3.0$ m season^{-1}. (b) Relationship between maximum deposition tolerance of vegetation ($\tau_{D\_physioMax}$) and foraging demand threshold, while $\tau_{E\_physioMax} = -2.5$ m season^{-1}. (c) Relationship between the maximum erosion tolerance of vegetation ($\tau_{E\_physioMax}$) and the forage demand threshold, while $\tau_{D\_physioMax} = 3.0$ m season^{-1}.

Fig. 17. Eco-geomorphic interaction zones during the first stage of a transforming dune driven by climatic impact. Simulation parameters: initial $BSF = 0.34$ ($t_0 = 80$ yrs.), $q = 20$ m^3 m^{-1} yr^{-1}, $\tau_{E\_physioMax} = -2.1$ m season^{-1}, $\tau_{D\_physioMax} = 2.9$ m season^{-1}, and $I_{climate} = -0.14$. Points *a*, *b*, *c*, and *d* reflect boundaries between zones along the transverse section at 250 m Eastings: zone 1 (dune edge - *a*), zone 2 (*a* - *b*), zone 3 (*b* - *c*), and zone 4 (*c* - *d*). The purple dashed square in bottom panel indicates the zoomed-in area of the upper panels.

Fig. 18. Time-evolution traces of topography (*H*) and vegetation effectiveness (*ρ*) in the four eco-geomorphic interaction zones during the first stage of a transforming dune driven by climatic impact (Fig.17). Points *a*, *b*, *c*, and *d* refer to the boundaries between the zones as shown in Fig.17. Each line/colour represents the time-evolution of a 1×1 m^2 cell along the transverse section. Colour gradation and arrows indicate traces of all the cells spanning from one boundary to the next.

Fig. 19. Eco-geomorphic interaction zones during the second stage of a transforming dune driven by climatic impact, continuing on from simulation shown in Fig.17. Simulation parameters and point labels same as caption to Fig.17.

Fig. 20. Time-evolution traces of topography (*H*) and vegetation effectiveness (*ρ*) in the four eco-geomorphic interaction zones during the second stage of a transforming dune driven by climatic impact (Fig.19). Points *a*, *b*, *c*, and *d* refer to the boundaries between the zones as shown in Fig.19. Each line/colour represents the time-evolution of a 1×1 m^2 cell along the transverse section. Colour gradation and arrows indicate traces of all the cells spanning from one boundary to the next.

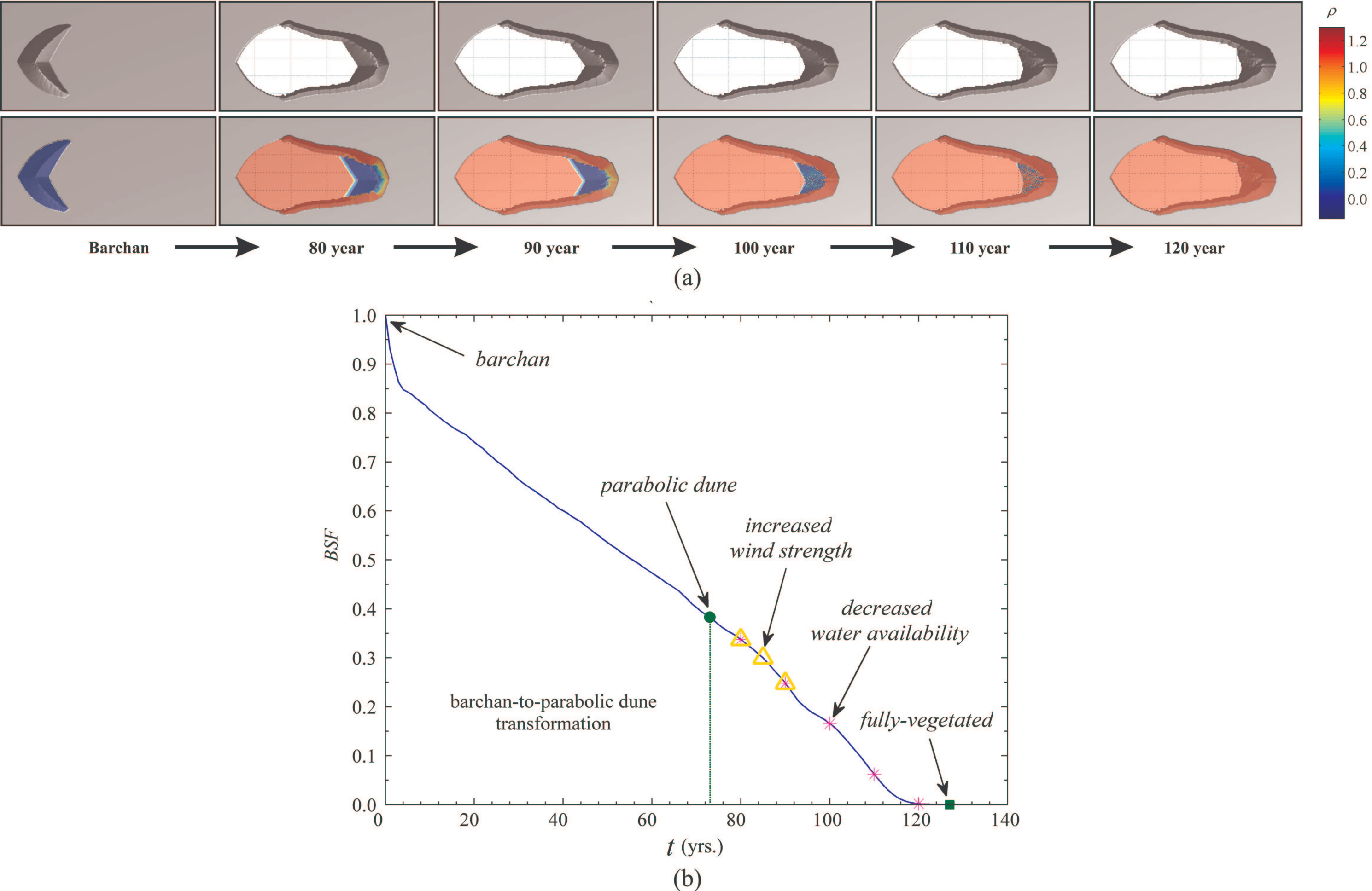
ρ
1.2
1.0
0.8
0.6
0.4
0.2
0.0
Barchan
80 year
90 year
100 year
110 year
120 year
(a)
1.0
0.9
0.8
0.7
0.6
0.5
0.4
0.3
0.2
0.1
0.0
BSF
0
20
40
60
80
100
120
140
t (yrs.)
barchan
parabolic dune
increased wind strength
decreased water availability
fully-vegetated
barchan-to-parabolic dune transformation
(b)

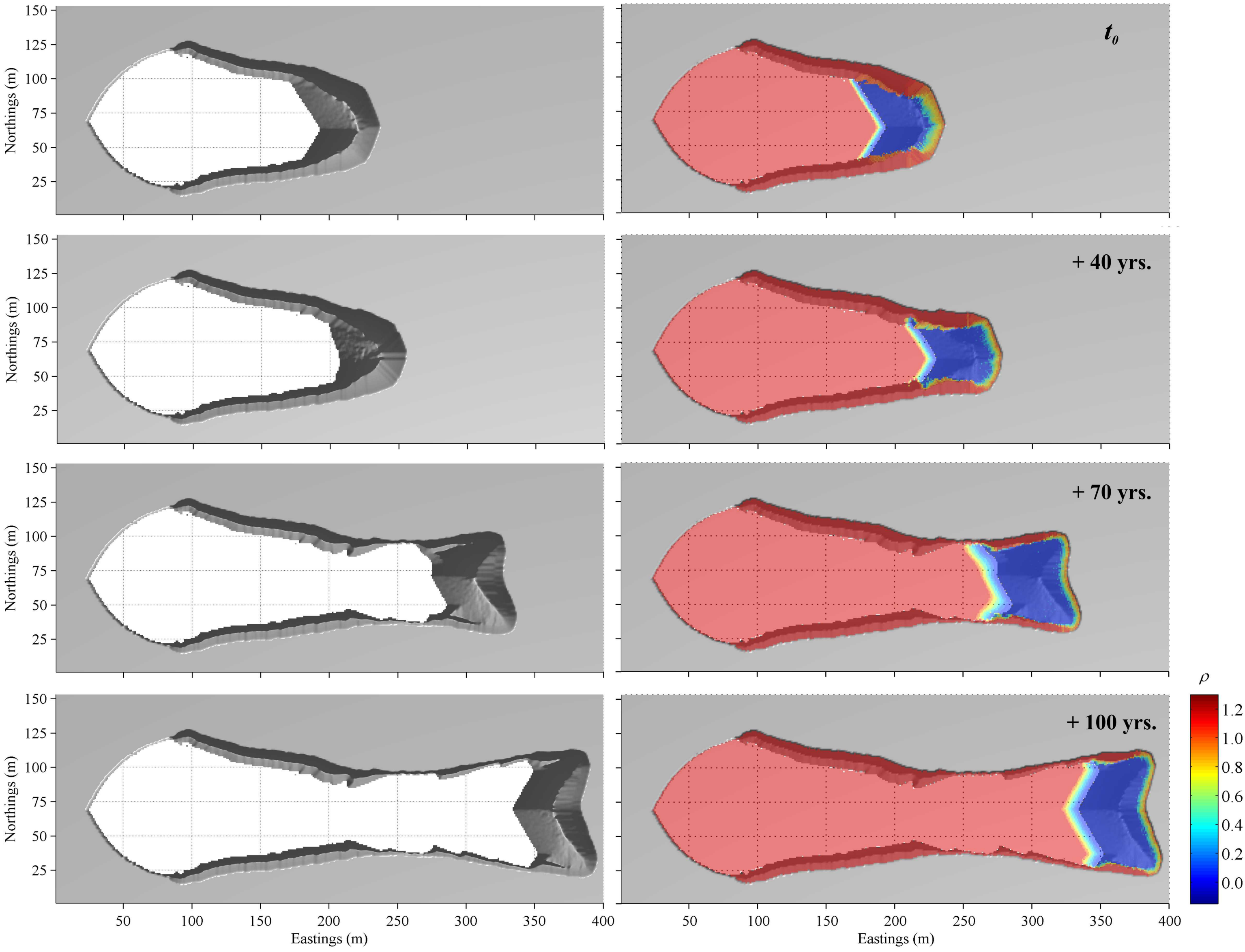
Northings (m)
150
125
100
75
50
25
Eastings (m)
50
100
150
200
250
300
350
400
t_0
+ 40 yrs.
+ 70 yrs.
+ 100 yrs.
ρ
1.2
1.0
0.8
0.6
0.4
0.2
0.0

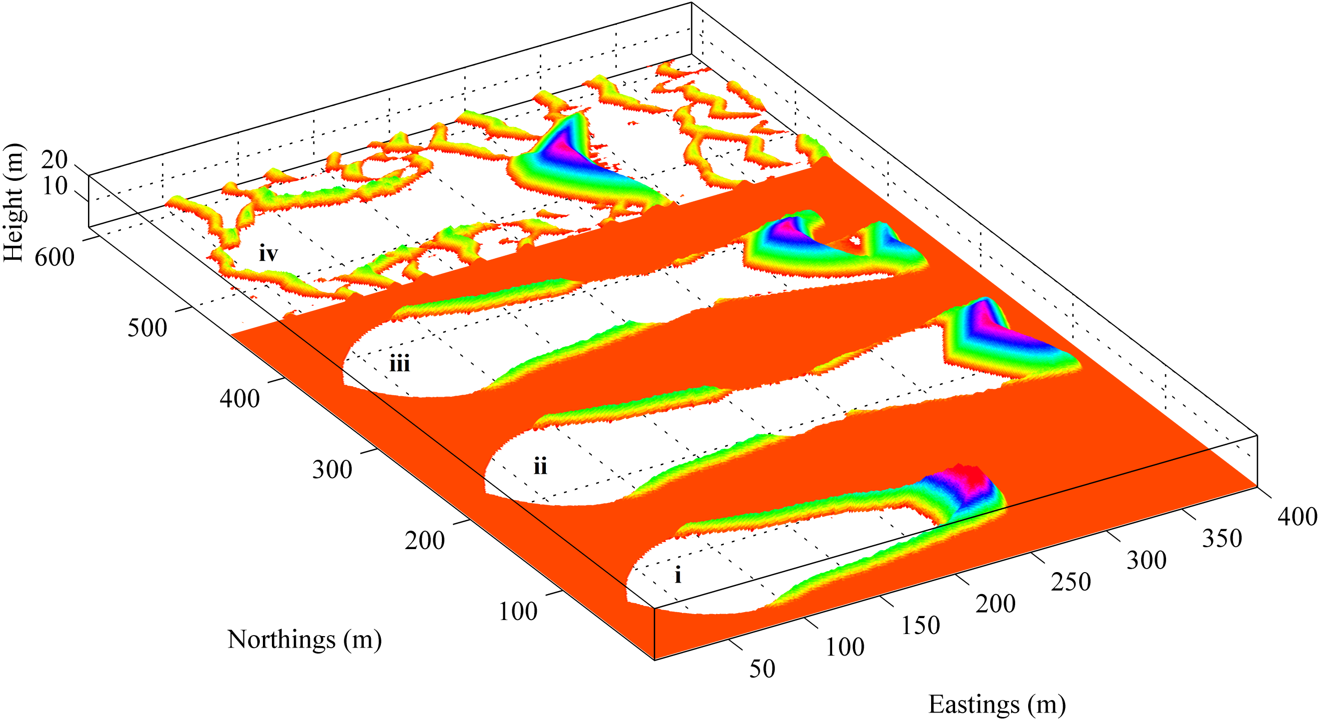
Height (m)
20
10
600
500
400
300
200
100
Northings (m)
50
100
150
200
250
300
350
400
Eastings (m)
i
ii
iii
iv

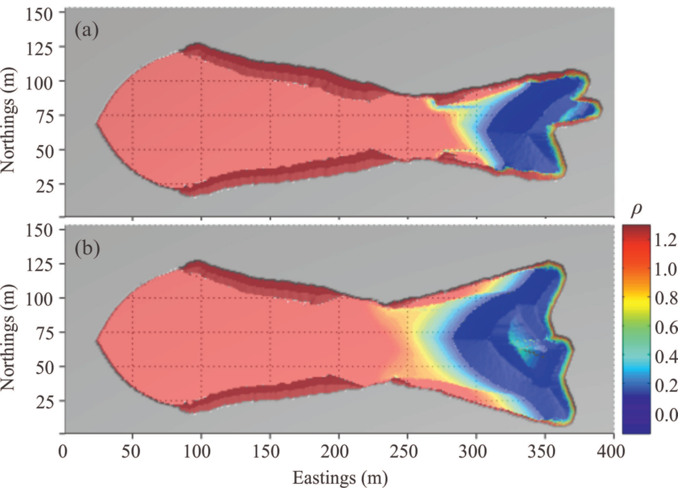
(a)
(b)
Northings (m)
150
125
100
75
50
25
Northings (m)
150
125
100
75
50
25
0
50
100
150
200
250
300
350
400
Eastings (m)
ρ
1.2
1.0
0.8
0.6
0.4
0.2
0.0

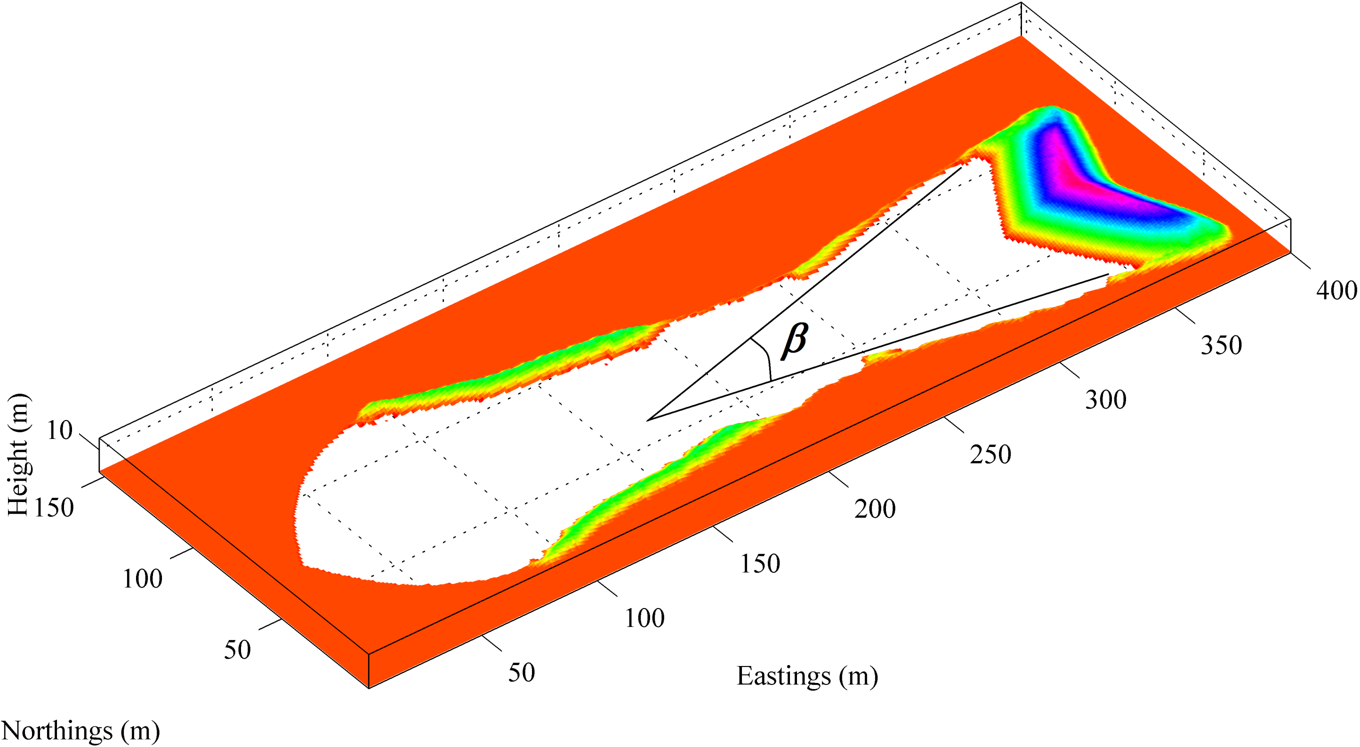
β
Height (m)
10
150
100
50
Northings (m)
50
100
150
200
250
300
350
400
Eastings (m)

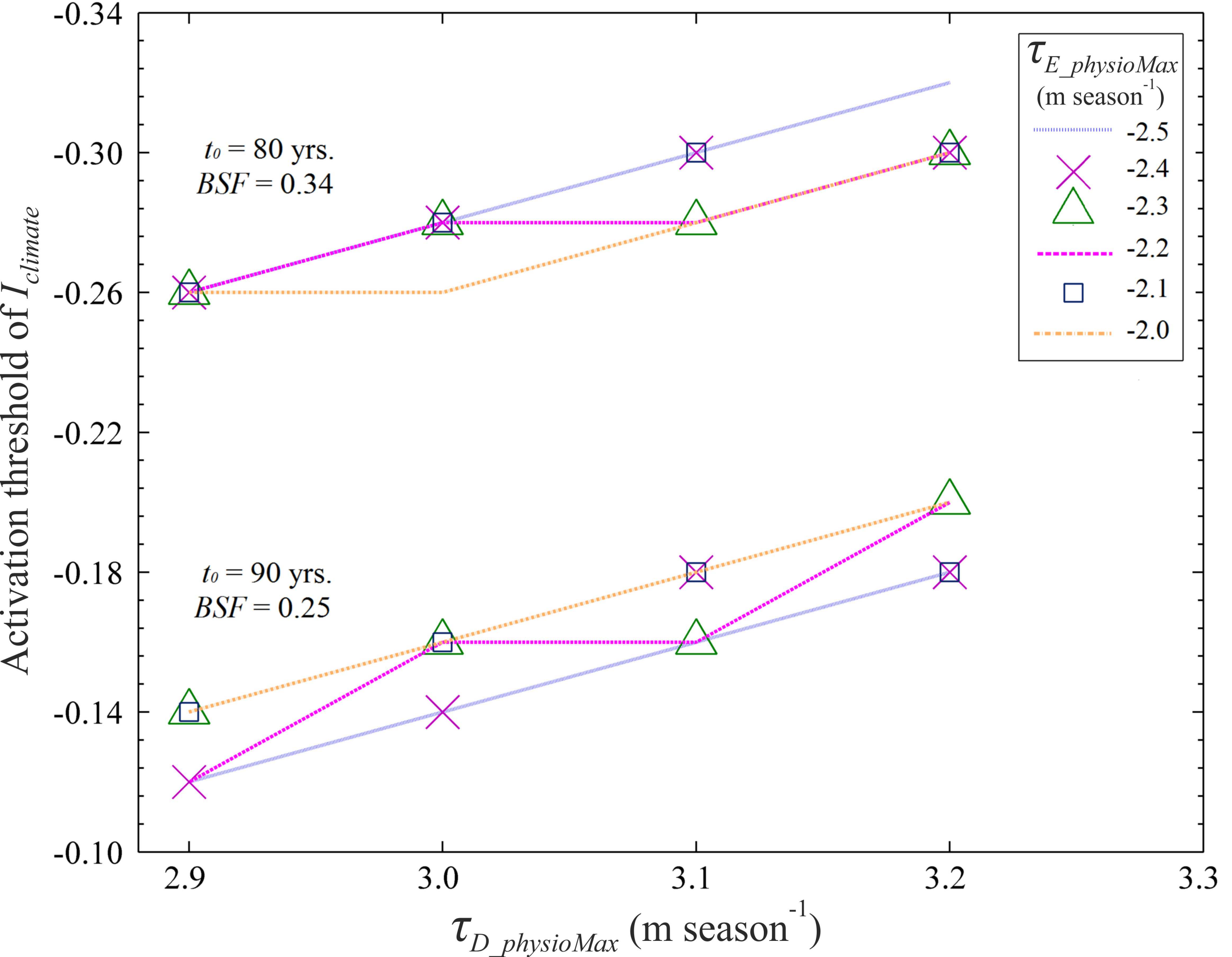
-0.34
-0.30
-0.26
-0.22
-0.18
-0.14
-0.10
2.9
3.0
3.1
3.2
3.3
Activation threshold of $I_{climate}$
$\tau_{D\_physioMax}$ (m season^{-1})
t_0 = 80 yrs.
BSF = 0.34
t_0 = 90 yrs.
BSF = 0.25
$\tau_{E\_physioMax}$
(m season^{-1})
-2.5
-2.4
-2.3
-2.2
-2.1
-2.0

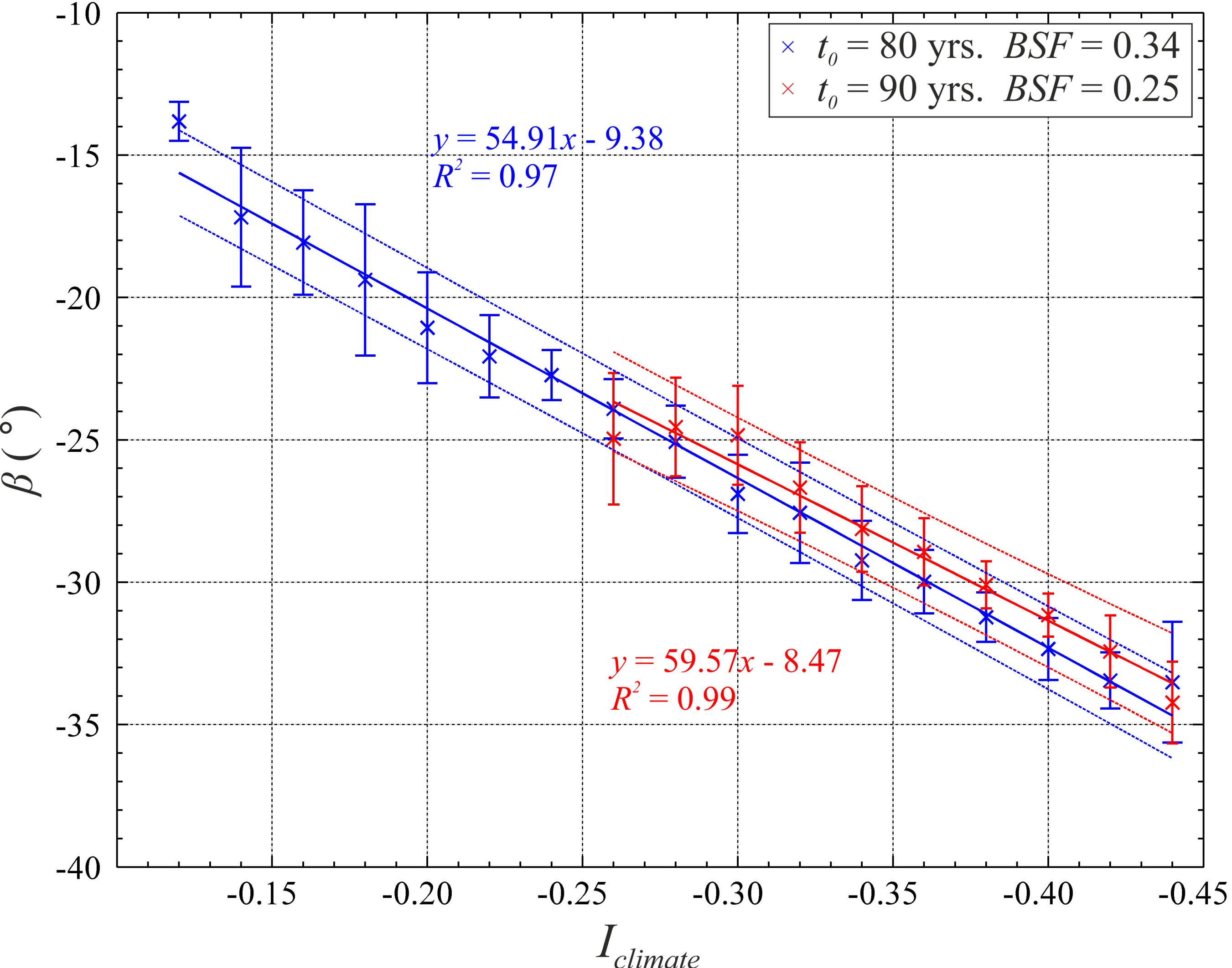

$t_0 = 80$ yrs. $BSF = 0.34$
$t_0 = 90$ yrs. $BSF = 0.25$
$y = 54.91x - 9.38$
$R^2 = 0.97$
$y = 59.57x - 8.47$
$R^2 = 0.99$
β (°)
$I_{climate}$
-10
-15
-20
-25
-30
-35
-40
-0.15
-0.20
-0.25
-0.30
-0.35
-0.40
-0.45

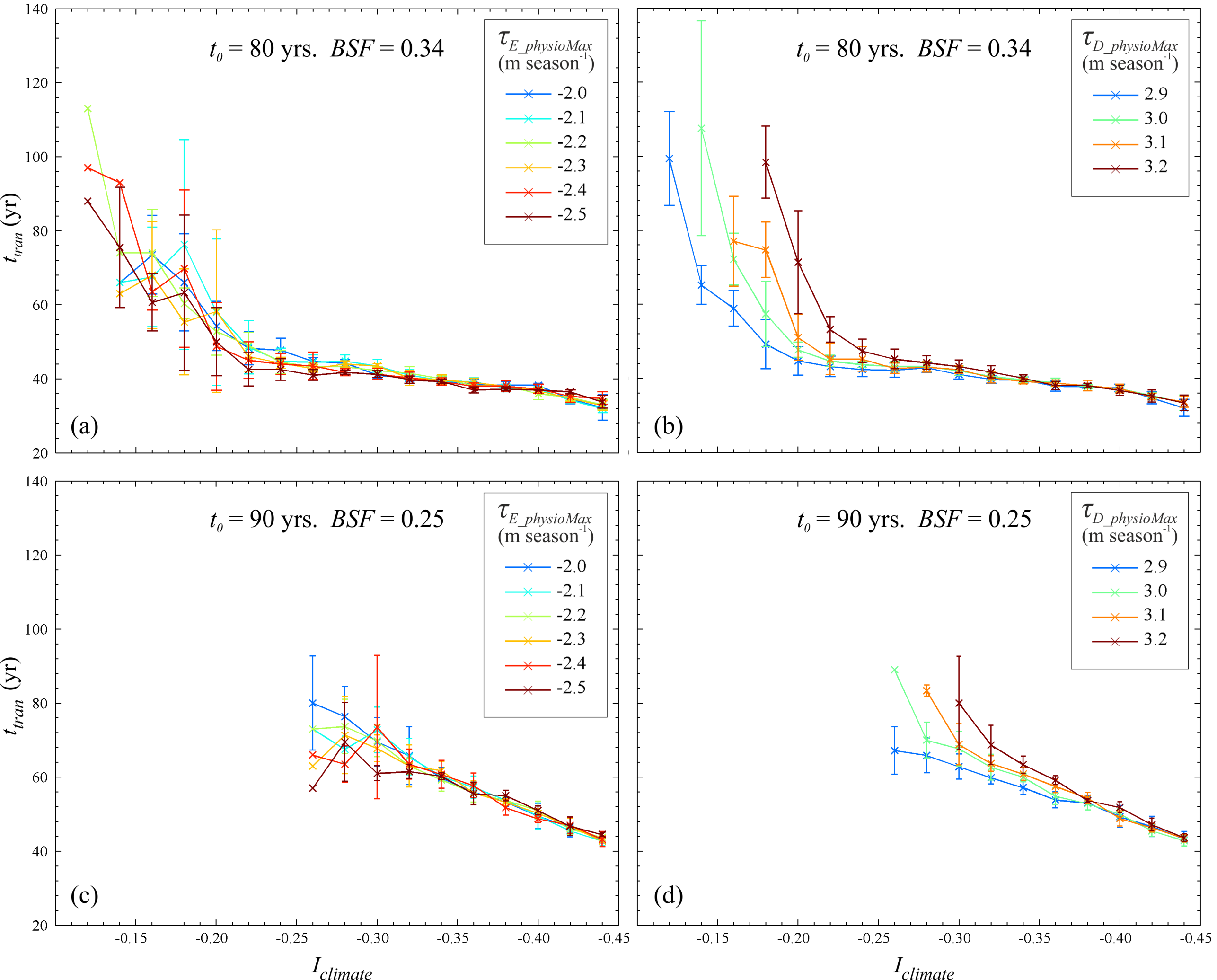
t_0 = 80 yrs. BSF = 0.34
$\tau_{E\_physioMax}$ (m season^{-1})
-2.0
-2.1
-2.2
-2.3
-2.4
-2.5
(a)
$\tau_{D\_physioMax}$ (m season^{-1})
2.9
3.0
3.1
3.2
(b)
t_0 = 90 yrs. BSF = 0.25
(c)
(d)
t_{tran} (yr)
140
120
100
80
60
40
20
-0.15
-0.20
-0.25
-0.30
-0.35
-0.40
-0.45
$I_{climate}$

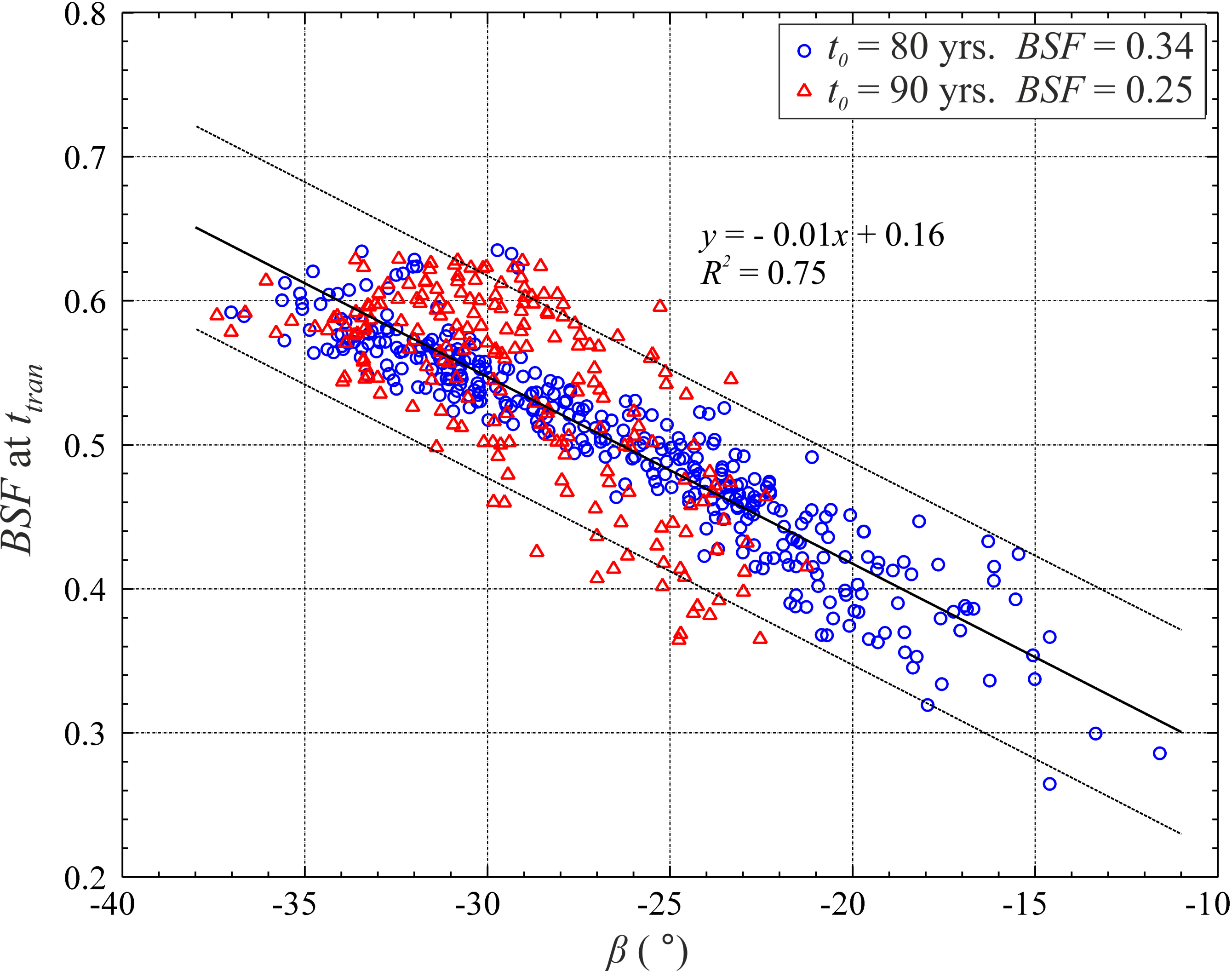

0.8
0.7
0.6
0.5
0.4
0.3
0.2
-40
-35
-30
-25
-20
-15
-10
BSF at t_tran
β (°)
○ t_0 = 80 yrs. BSF = 0.34
△ t_0 = 90 yrs. BSF = 0.25
y = - 0.01x + 0.16
R^2 = 0.75

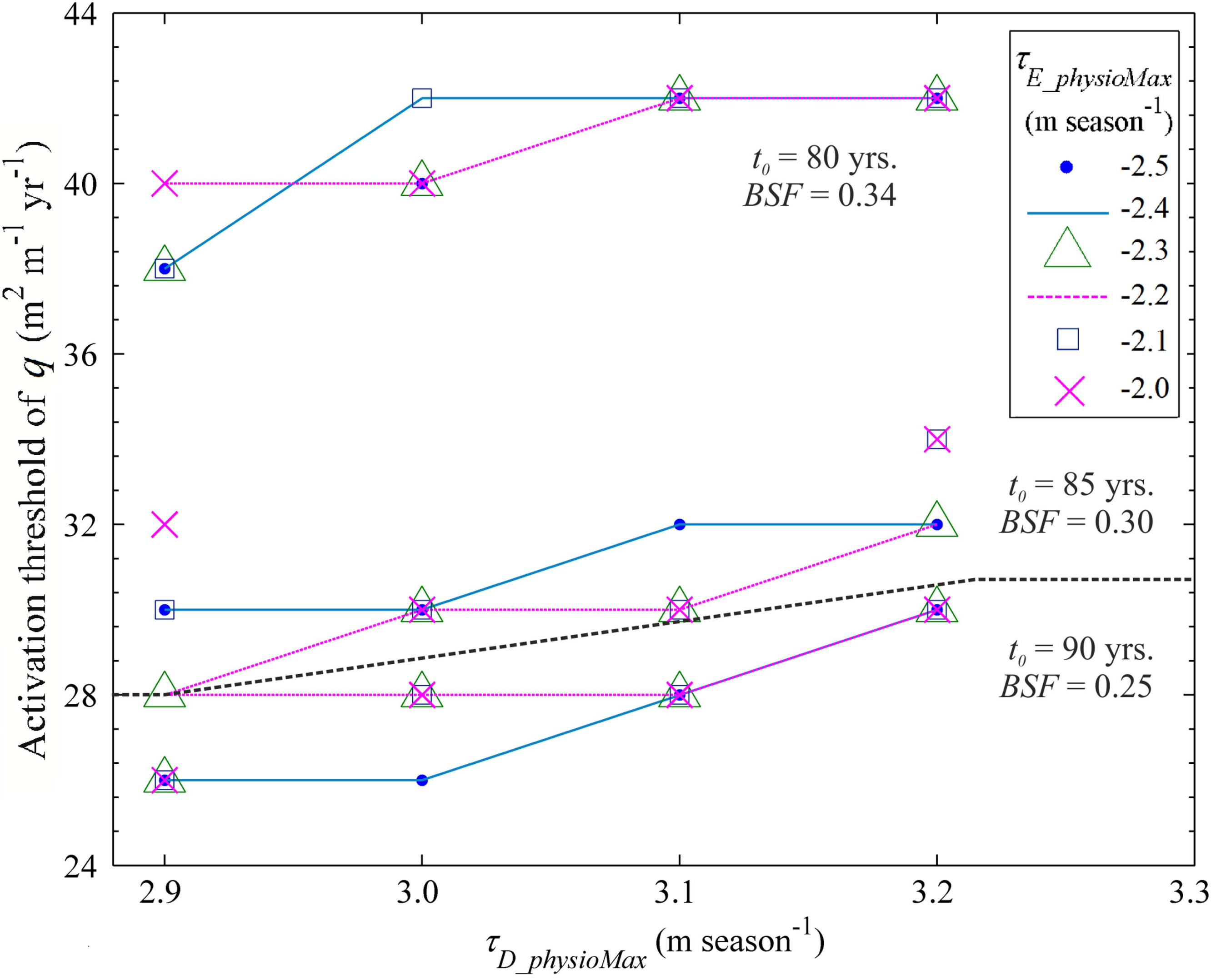

Activation threshold of q (m^2 m^{-1} yr^{-1})
44
40
36
32
28
24
2.9
3.0
3.1
3.2
3.3
$\tau_{D\_physioMax}$ (m $season^{-1}$)
$\tau_{E\_physioMax}$ (m $season^{-1}$)
-2.5
-2.4
-2.3
-2.2
-2.1
-2.0
t_0 = 80 yrs.
BSF = 0.34
t_0 = 85 yrs.
BSF = 0.30
t_0 = 90 yrs.
BSF = 0.25

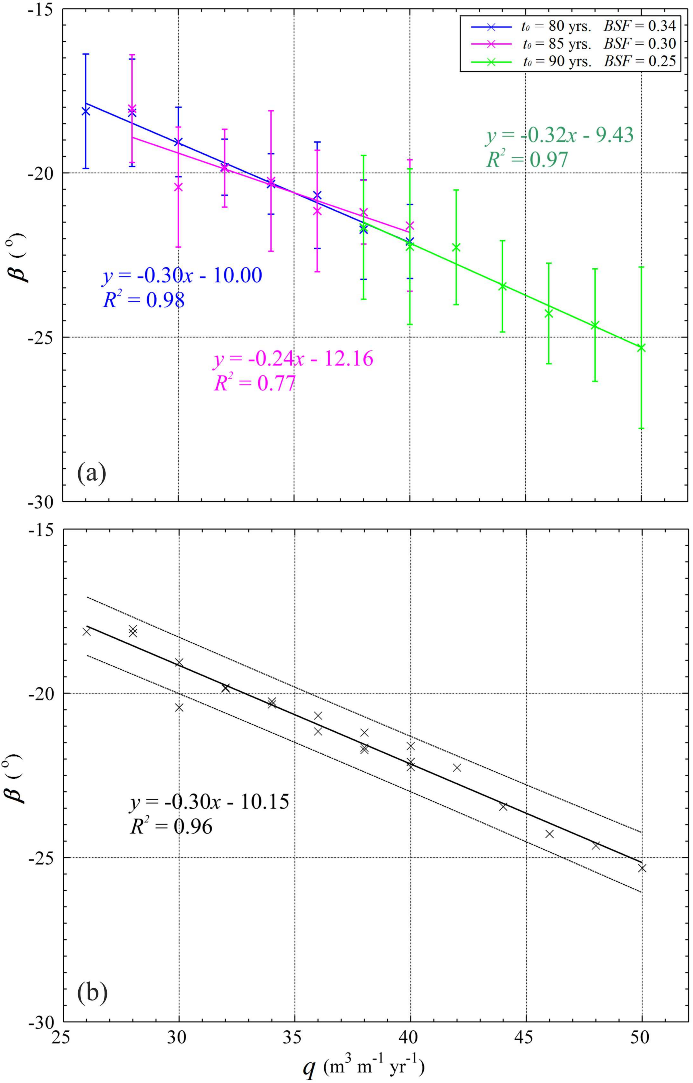
-15
-20
-25
-30
t_0 = 80 yrs. BSF = 0.34
t_0 = 85 yrs. BSF = 0.30
t_0 = 90 yrs. BSF = 0.25
y = -0.32x - 9.43
R^2 = 0.97
y = -0.30x - 10.00
R^2 = 0.98
y = -0.24x - 12.16
R^2 = 0.77
(a)
β (°)
-15
-20
-25
-30
y = -0.30x - 10.15
R^2 = 0.96
(b)
β (°)
25
30
35
40
45
50
q (m^3 m^{-1} yr^{-1})

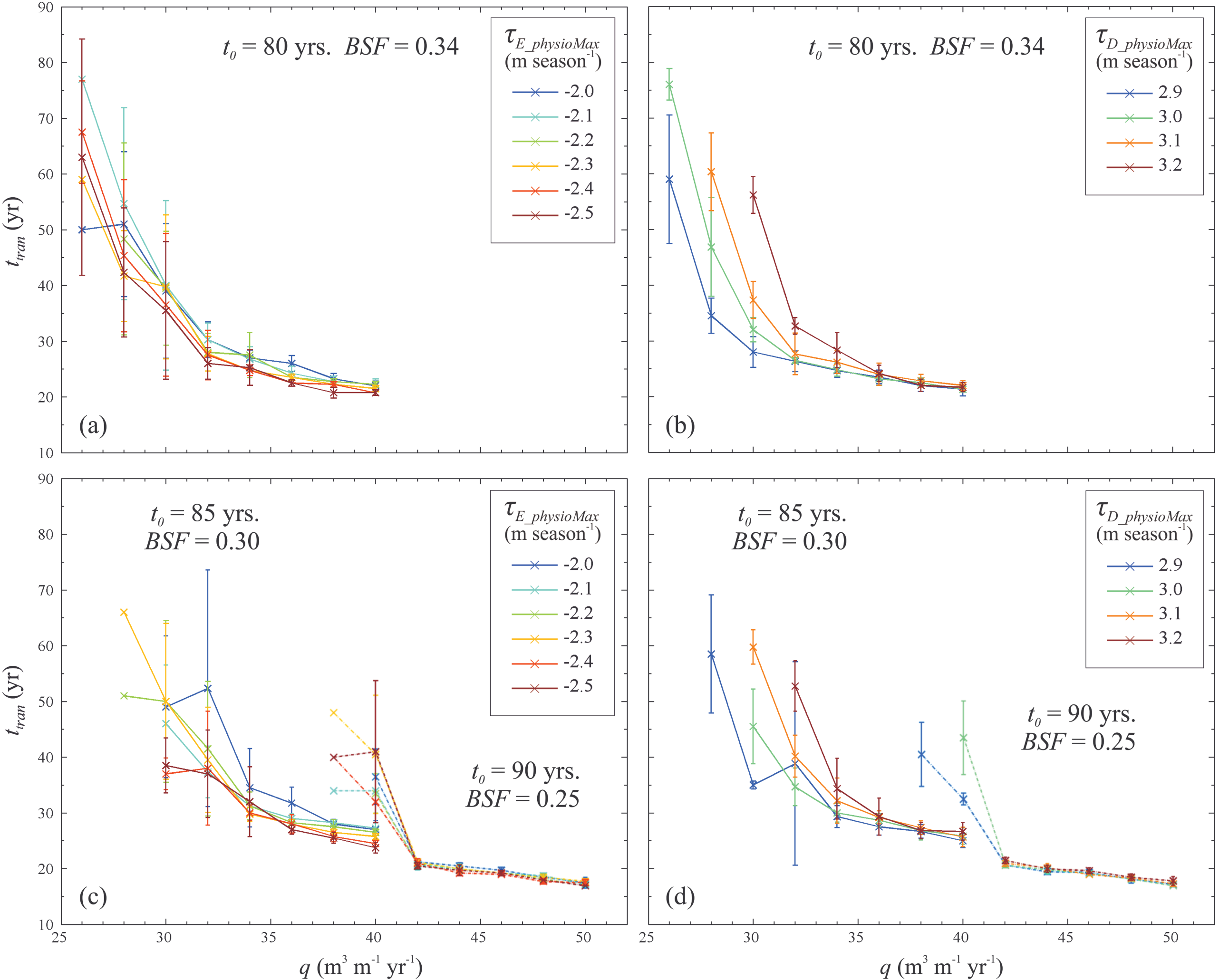
$t_0 = 80$ yrs. $BSF = 0.34$
$\tau_{E\_physioMax}$ (m season^{-1})
-2.0
-2.1
-2.2
-2.3
-2.4
-2.5
(a)
$t_0 = 80$ yrs. $BSF = 0.34$
$\tau_{D\_physioMax}$ (m season^{-1})
2.9
3.0
3.1
3.2
(b)
$t_0 = 85$ yrs. $BSF = 0.30$
$t_0 = 90$ yrs. $BSF = 0.25$
(c)
(d)
t_{tran} (yr)
q (m^3 m^{-1} yr^{-1})
10
20
30
40
50
60
70
80
90
25
30
35
40
45
50

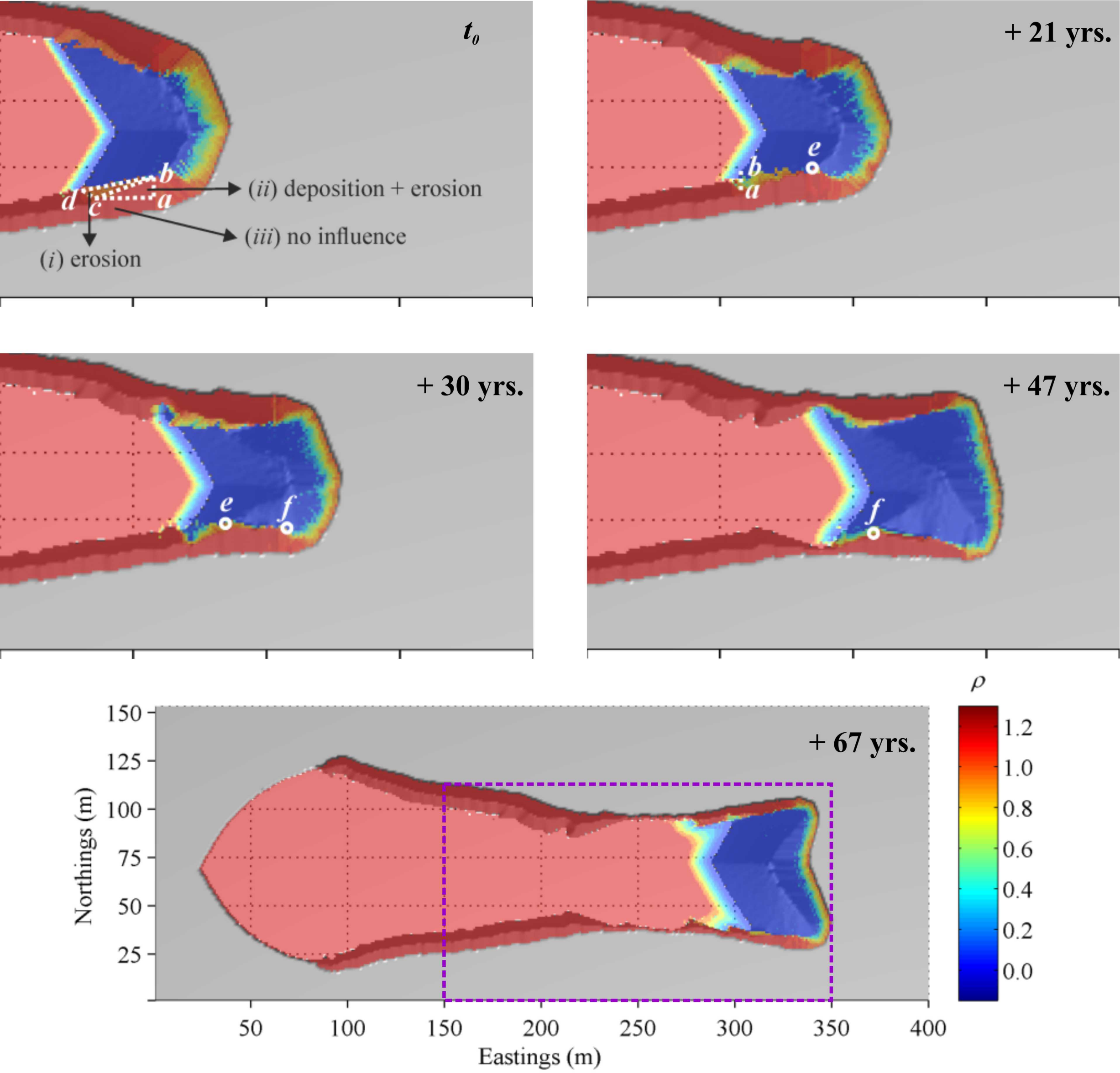
t_0
+ 21 yrs.
+ 30 yrs.
+ 47 yrs.
+ 67 yrs.
a
b
c
d
e
f
(ii) deposition + erosion
(iii) no influence
(i) erosion
ρ
1.2
1.0
0.8
0.6
0.4
0.2
0.0
Northings (m)
150
125
100
75
50
25
Eastings (m)
50
100
150
200
250
300
350
400

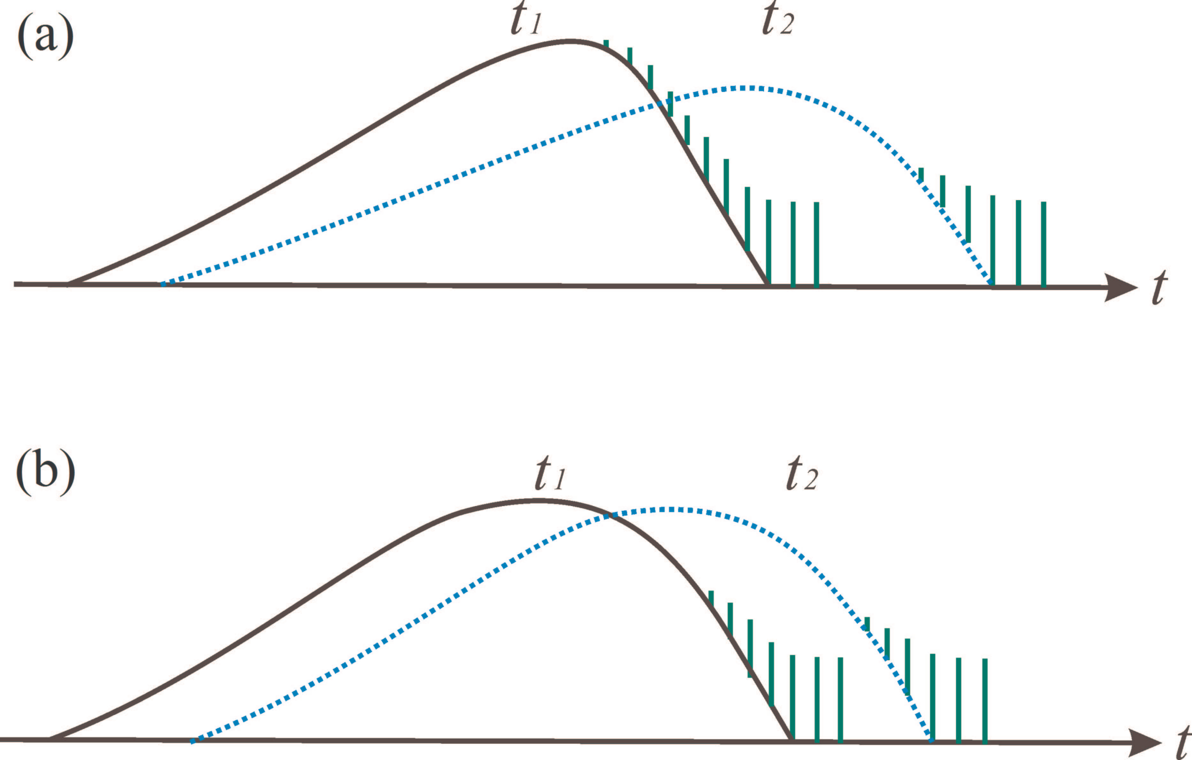
(a)
t1
t2
t
(b)
t1
t2
t

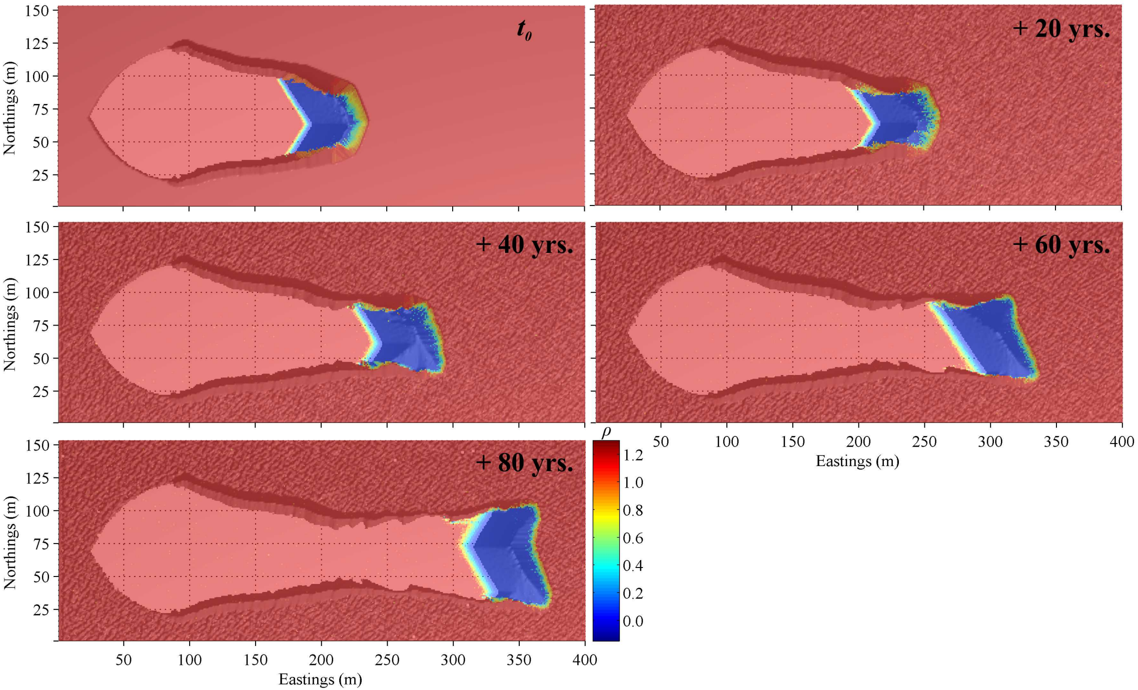

t_0
+ 20 yrs.
+ 40 yrs.
+ 60 yrs.
+ 80 yrs.
Northings (m)
150
125
100
75
50
25
Eastings (m)
50
100
150
200
250
300
350
400
ρ
1.2
1.0
0.8
0.6
0.4
0.2
0.0

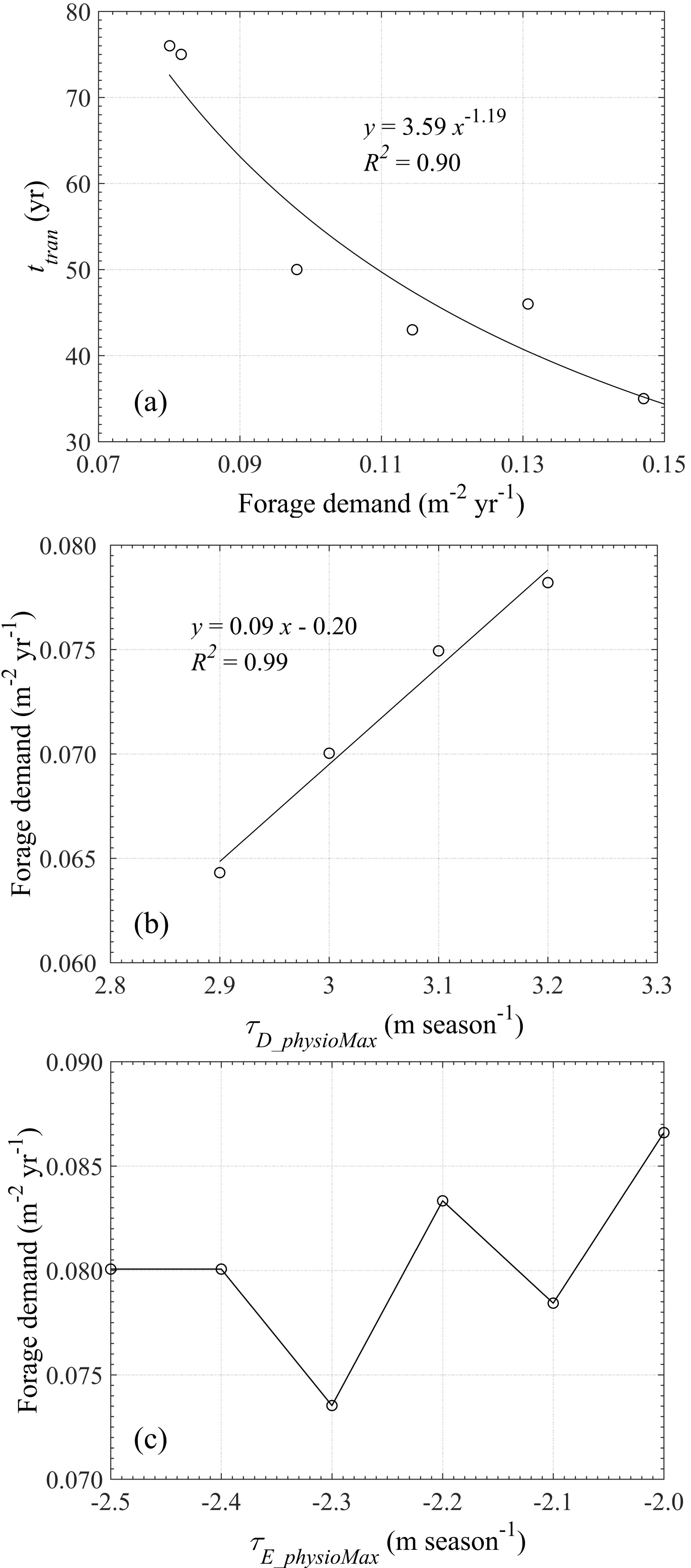
80
70
60
50
40
30
t_{tran} (yr)
$y = 3.59\ x^{-1.19}$
$R^2 = 0.90$
(a)
0.07
0.09
0.11
0.13
0.15
Forage demand (m^{-2} yr^{-1})
0.080
0.075
0.070
0.065
0.060
Forage demand (m^{-2} yr^{-1})
$y = 0.09\ x - 0.20$
$R^2 = 0.99$
(b)
2.8
2.9
3
3.1
3.2
3.3
$\tau_{D\_physioMax}$ (m season^{-1})
0.090
0.085
0.080
0.075
0.070
Forage demand (m^{-2} yr^{-1})
(c)
-2.5
-2.4
-2.3
-2.2
-2.1
-2.0
$\tau_{E\_physioMax}$ (m season^{-1})

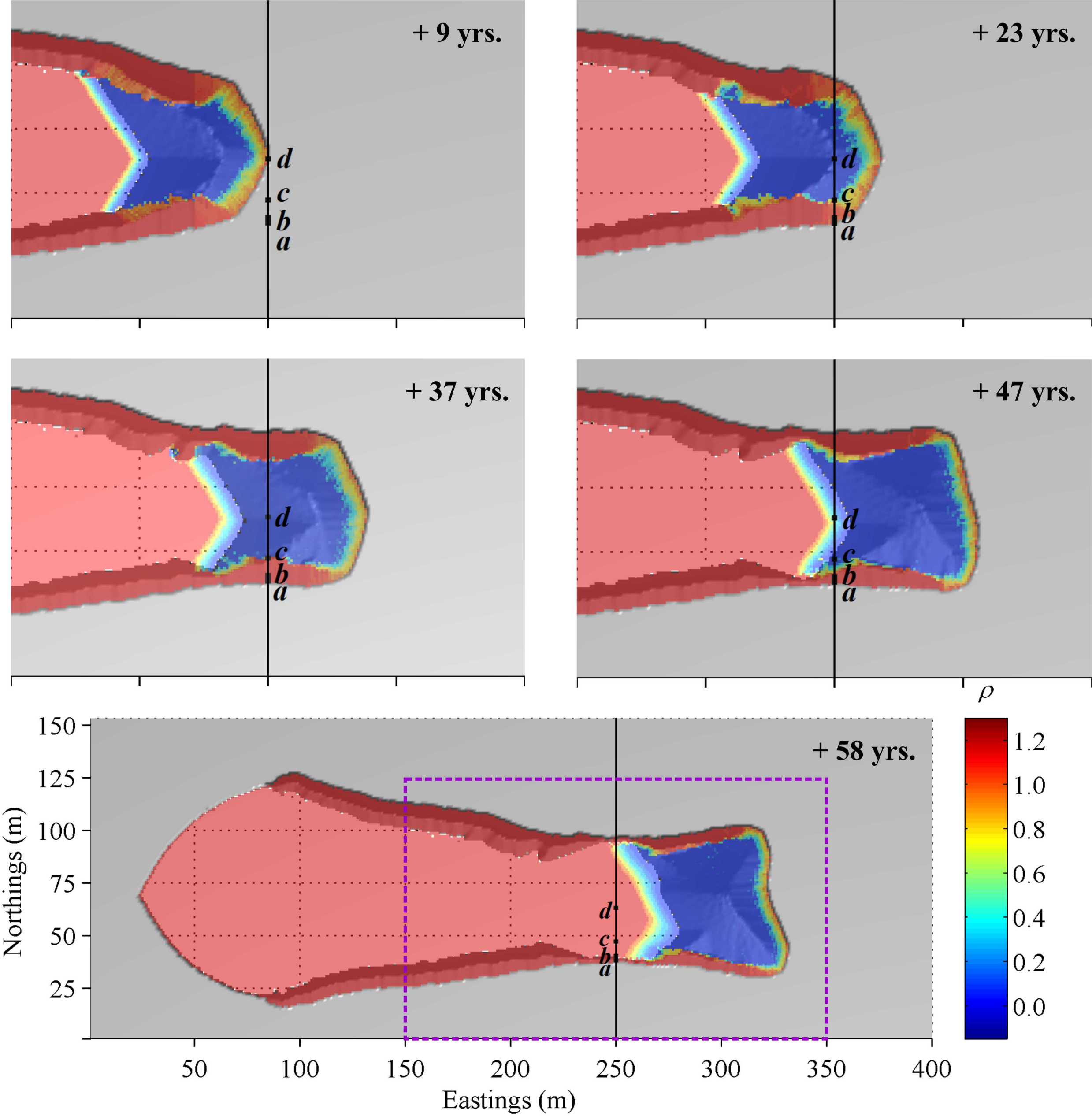
+ 9 yrs.
+ 23 yrs.
+ 37 yrs.
+ 47 yrs.
+ 58 yrs.
a
b
c
d
ρ
1.2
1.0
0.8
0.6
0.4
0.2
0.0
Northings (m)
150
125
100
75
50
25
Eastings (m)
50
100
150
200
250
300
350
400

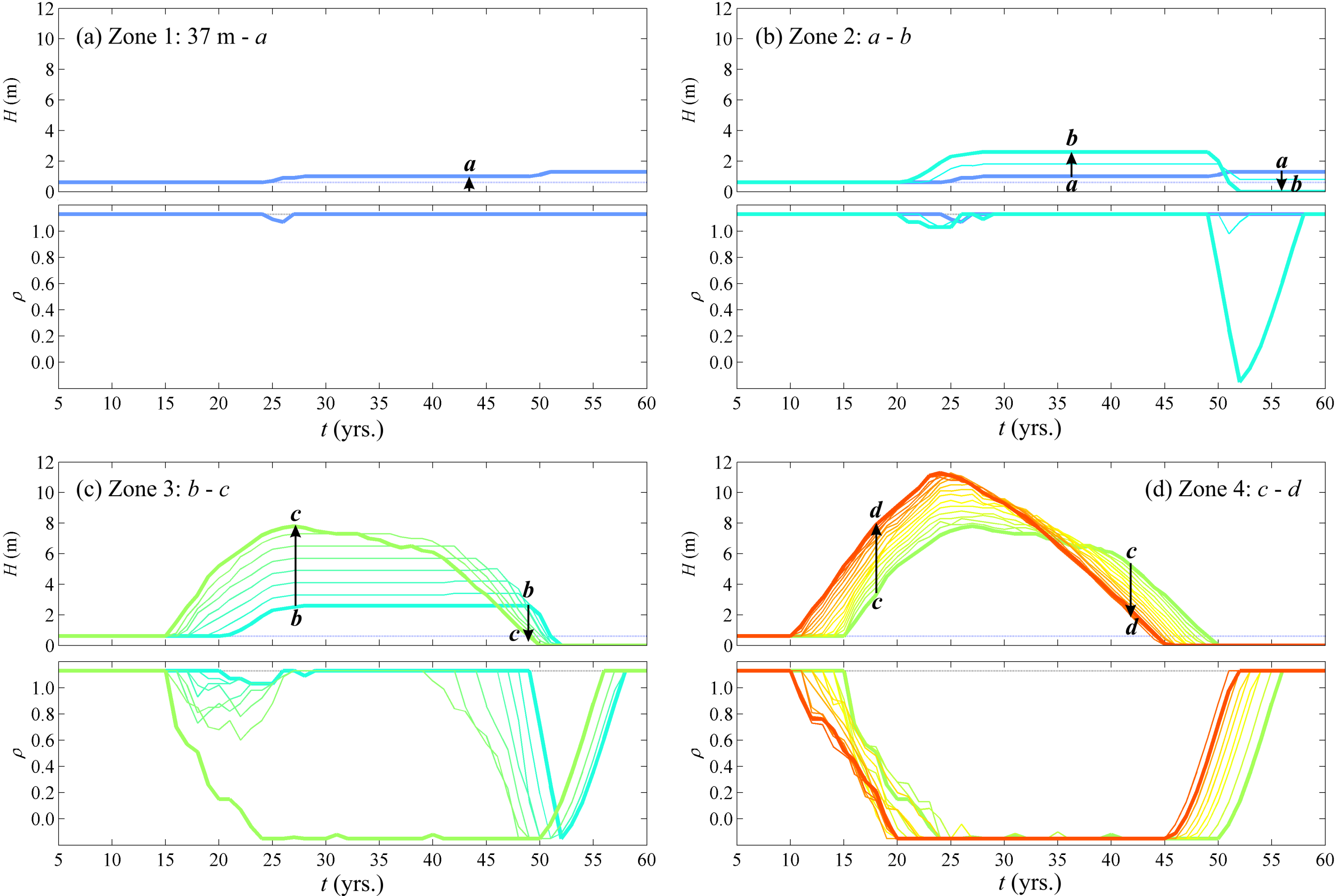
(a) Zone 1: 37 m - *a*
(b) Zone 2: *a* - *b*
(c) Zone 3: *b* - *c*
(d) Zone 4: *c* - *d*
H (m)
ρ
t (yrs.)
0
2
4
6
8
10
12
0.0
0.2
0.4
0.6
0.8
1.0
5
10
15
20
25
30
35
40
45
50
55
60
a
b
c
d

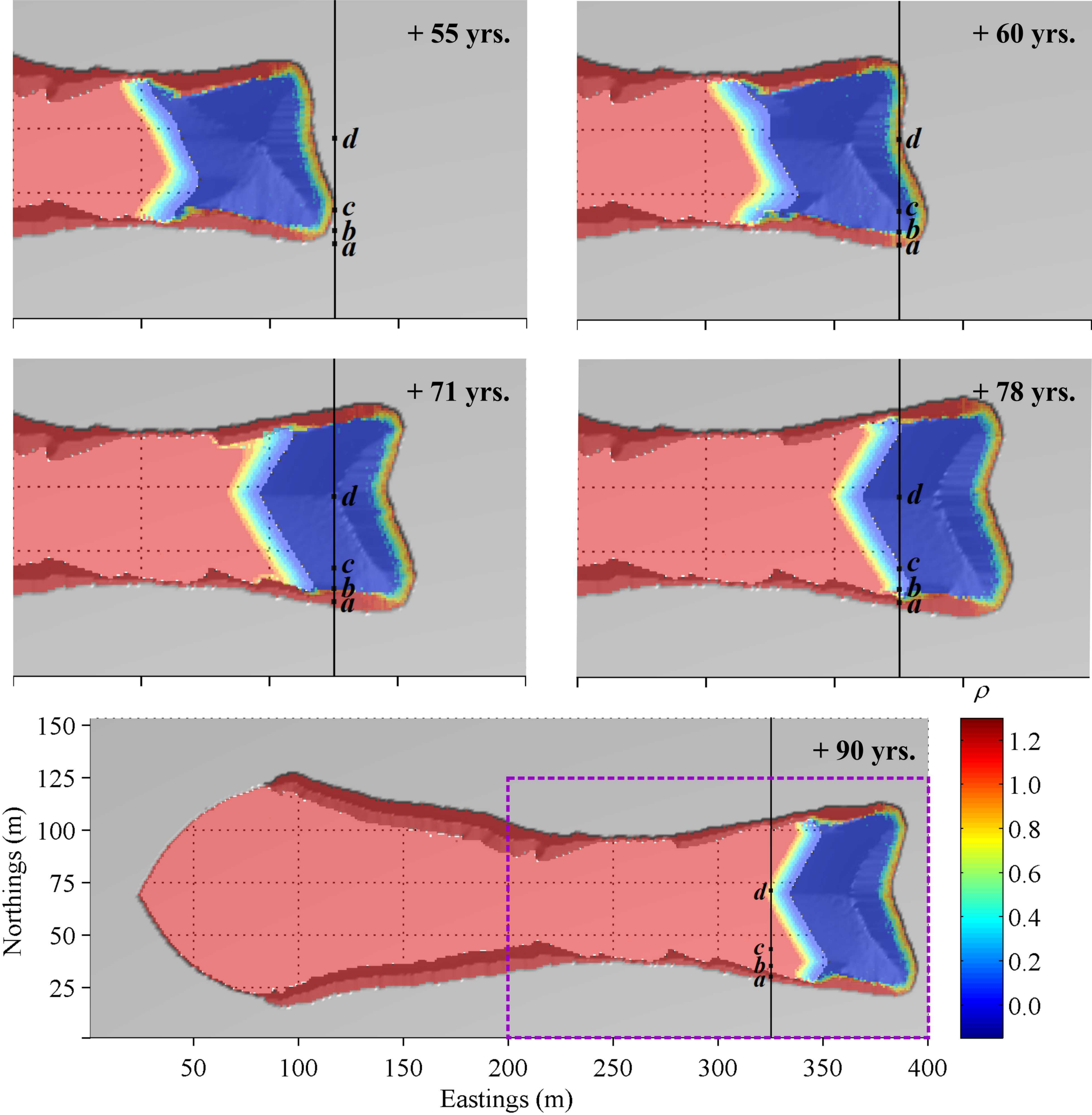

+ 55 yrs.
+ 60 yrs.
+ 71 yrs.
+ 78 yrs.
+ 90 yrs.
d
c
b
a
ρ
1.2
1.0
0.8
0.6
0.4
0.2
0.0
150
125
100
75
50
25
Northings (m)
50
100
150
200
250
300
350
400
Eastings (m)

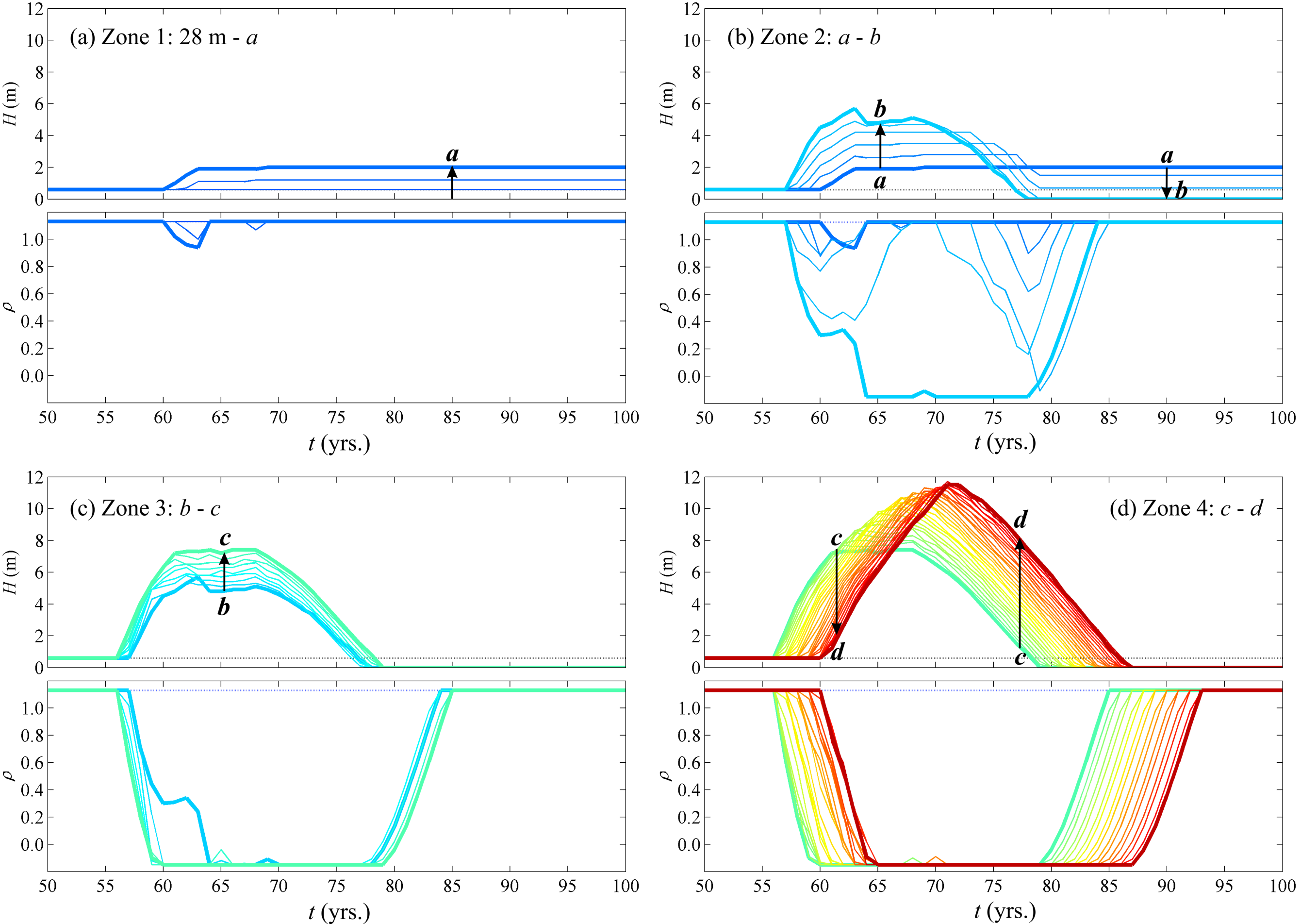
(a) Zone 1: 28 m - a
(b) Zone 2: a - b
(c) Zone 3: b - c
(d) Zone 4: c - d
H (m)
ρ
t (yrs.)
a
b
c
d
0
2
4
6
8
10
12
0.0
0.2
0.4
0.6
0.8
1.0
50
55
60
65
70
75
80
85
90
95
100